creative commons
COMMONS DEED

저작자표시-비영리-변경금지 2.0 대한민국

이용자는 아래의 조건을 따르는 경우에 한하여 자유롭게

- 이 저작물을 복제, 배포, 전송, 전시, 공연 및 방송할 수 있습니다.

다음과 같은 조건을 따라야 합니다:

저작자표시. 귀하는 원저작자를 표시하여야 합니다.

비영리. 귀하는 이 저작물을 영리 목적으로 이용할 수 없습니다.

변경금지. 귀하는 이 저작물을 개작, 변형 또는 가공할 수 없습니다.

- 귀하는, 이 저작물의 재이용이나 배포의 경우, 이 저작물에 적용된 이용허락조건을 명확하게 나타내어야 합니다.
- 저작권자로부터 별도의 허가를 받으면 이러한 조건들은 적용되지 않습니다.

저작권법에 따른 이용자의 권리는 위의 내용에 의하여 영향을 받지 않습니다.

이것은 이용허락규약(Legal Code)을 이해하기 쉽게 요약한 것입니다.

Disclaimer

dCollection

[UCI]I804:48009-200000502176

EFFICIENT PILOT ASSIGNMENT AND POWER ALLOCATION FOR ENHANCING ENERGY AND SPECTRAL EFFICIENCY IN MASSIVE MIMO SYSTEMS

DISSERTATION

for the Degree of

DOCTOR OF PHILOSOPHY
(Electrical, Electronic and Computer Engineering)

HIEU TRONG DAO

MAY 2021

Efficient pilot assignment and power allocation for enhancing energy and spectral efficiency in massive MIMO systems

DISSERTATION

Submitted in Partial Fulfillment
of the Requirements for the
Degree of

DOCTOR OF PHILOSOPHY
(Electrical, Electronic and Computer Engineering)

at the

UNIVERSITY OF ULSAN

by

Hieu Trong Dao
Supervisor: Professor Sunghwan Kim
May 2021

Publication No._____

©2021 - Hieu Trong Dao

All rights reserved.

Efficient pilot assignment and power allocation for enhancing energy and spectral efficiency in massive MIMO systems

Approved by Supervisory Committee:

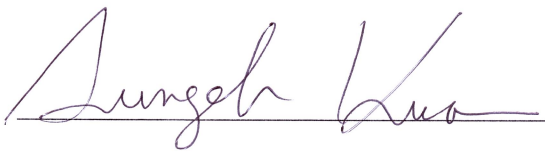

Prof. Sungoh Kwon, *chair*

Prof. Kyoung-Young Song

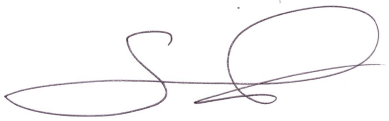

Prof. Jiho Song

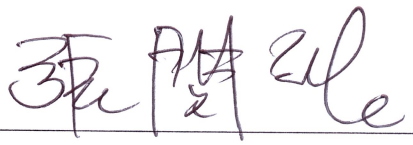

Prof. Min-Ho Jang

Prof. Sunghwan Kim, *adviser*

May, 2021

VITA

Hieu Trong Dao was born in Hanoi, Vietnam on November 30, 1991. He received the B.S. degree from the Hanoi University of Science and Technology, in 2014. After graduation, he was a software engineer at Samsung Vietnam Mobile Research and Development Center, from 2014 to 2015, and a mobile network engineer at Viettel Group, Vietnam, from 2015 to 2016. In September 2016, he started pursuing the combined M.S. and Ph.D. degrees as a researcher at University of Ulsan, South Korea under the supervision of professor Sunghwan Kim. His main research interests include 5G communication, massive MIMO, and modulation techniques.

Dedicated to my family and specially my wife

for their belief, love and support

ACKNOWLEDGMENTS

This thesis may not have been possible without unconditioned support of many people. I would like to thank people who have contributed to this thesis.

First and foremost, I would like to express my sincere gratitude to my advisor, Prof. Sunghwan Kim, for giving me the chance to be a member of Coding and Information Theory (CIT) lab and for his great guidance in weekly meeting which helped me to complete my work. I really appreciate his full support, constant encouragement, and advices both in research and in life.

I would also like to thank my committee members for many useful interactions and for contributing their broad perspective in redefining the ideas in this dissertation. I am grateful to my lab mates and friends in University of Ulsan for their sincerely friendship, enthusiastic help, and cheerfulness during my stay in Ulsan, Korea.

I am very much grateful to University of Ulsan for giving me such a wonderful research environment and financial support (through BK21+ programs). UOU gave me the chance to conduct a number of useful courses with excellent instructors that will give me a way to think and work properly in the rest of my life.

Last but not least, I am deeply indebted to my parents and my wife for their love and unconditioned supports. Without their love, I would not be who I am today.

ABSTRACT

Efficient pilot assignment and power allocation for enhancing energy and spectral efficiency in massive MIMO systems

by: **Hieu Trong Dao**

Advisor: **Prof. Sunghwan Kim**

Submitted in Partial Fulfillment of the Requirements for the Degree of Doctor of Philosophy (Electrical, Electronic and Computer Engineering)

May 2021

Massive multiple-input-multiple-output (MIMO) has been considered as a promising transmission technique for future wireless networks (5G and beyond) since it has the ability to significantly improve both spectral efficiency and energy efficiency of the wireless systems. Moreover, base stations only need to use simple linear signal processing technique for both uplink signal detection and downlink pre-coding, such as zero forcing or maximum ratio, but they still are able to achieve nearly optimal performance. The huge potential of massive MIMO systems is undeniable; however, there are many aspects of massive MIMO systems should be deeply investigated and improved so that this technique can meet the huge demand for data transmission in the near future.

Pilot contamination (PC) is one of the main drawbacks of massive MIMO systems. This PC happens due to the lack of resources since massive MIMO systems

consist of many users and huge number of base station antennas. PC degrades the channel estimation quality, and eventually degrades spectral and energy efficiency of the massive MIMO system. Therefore, this thesis investigates some methods to mitigate the PC problems and also to improve the energy efficiency of the massive MIMO systems. Specifically, this thesis firstly focuses on how to allocate pilot sequence and pilot power to each user in a smart way to degrade the effect of PC problem, or in other words, to improve the spectral efficiency of the systems. Moreover, massive MIMO system consists of many users and a huge number of BS antennas. Therefore, using power efficiently is very important issue. Inspired by that, this thesis also investigates methods to improve the energy efficiency of the massive MIMO systems.

Contents

Chapter 1

Introduction

1.1 Cellular network and motivation to massive MIMO

In 1947, researchers at Bell Labs proposed new idea on a cellular network topology [1]. Specifically, a cellular network is deployed over an area, which is divided into many samller area called cells. Cells operate individually and independenly using a base station (BS), which usually is located at the cell center. Cells can be regarded as an element of network equipment that facilitates wireless communication between a device and the system. The concept of cellular network was further improved and analyzed over the next decades [2], [3] and then deployed in practice. Without doubt, cellular networks were major breakthroughs and have been the main media to deliver wireless services.

Generally, a cellular network contains a set of BSs and a set of user equipments

(UEs). UEs are connected to their corresponding BS, which provides service to them. The downlink (DL) refers to signals sent from the BSs to their corresponding UEs, and the uplink (UL) refers to data transmissions from the UEs to their corresponding BS. An illustration of a cellular network is presented in Figure 1.1.

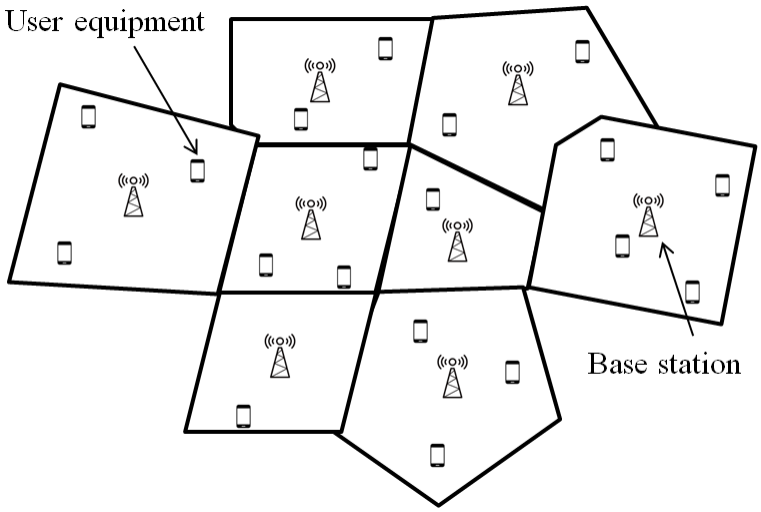

Figure 1.1: A general cellular network.

During the last few years, demand of data traffic transmission has increased exponentially due to the significant growth of smartphones, laptops, tablets and many other wireless devices. Global mobile data traffic has reached to more than 20 exabytes per month by 2020, which has increased more than 8 times compared to 2014. Moreover, the number of wireless devices and connections are expected to grow much faster in the near future, and new technologies are required to meet this huge demand. In cellular networks, one important parameter to consider is wireless throughput (bit/s/km^2). This parameter can be defined as

$$\text{Throughput} = \text{Bandwidth [Hz]} * \text{Cell density [cells/km}^2\text{]} * \text{Spectral efficiency [bit/s/Hz]}. \tag{1.1}$$

Accordingly, there are three ways to improve the area throughput of a cellular network:

- Use more bandwidth;
- Densify the network by deploying more BSs on the same area;
- Improve the spectral efficiency (SE).

The first option is to increase the bandwidth. However, bandwidth is a global and limited resource. Therefore, we can only use millimeter wavelength band (30-300 GHz or higher). Unfortunately, due to the characteristics of high frequency signals, these bandwidths can only be used for short-range applications. In conclusion, to secure more larger bandwidth is impractical. The second option is to densify the cellular network by deploying more BS per area unit, and it is clearly not practical. Finally, major improvements in SE are needed and massive multiple-input multiple-output (massive MIMO) technique is a promissing technique to solve this problem.

1.2 Spectral efficiency definition

We consider a communication channel with badwidth of B Hz. According to Nyquist-Shannon sampling theorem, the band-limited communication signal that is transmitted over this channel is determined by 2B real-valued equal-spaced samples

per second [4]. if the baseband representation of the signal is complex, B complex-valued samples per second is the more suitable quantity [5]. The B samples are the degrees of freedom available for creating the communication signal. Consequently, SE is the amount of information that can be transmitted reliably per complex-valued sample.

In the view of coding information, SE of an encoding/decoding scheme is the average number of bits of information, per complex valued sample, that it can reliably transmit over the channel under consideration. it is obvious that SE is a deterministic number that can be calculated in bit per complex-valued sample. Since there are B samples per second, an equivalent unit of the SE is bit per second per Hertz (bit/s/Hz). For fading channels, which change over time, SE can be considered as the average number of bit/s/Hz over the fading realizations. We often consider SE of a channel between an UE and a BS as channel capacity. For simplicity, we refer as the user SE or user capacity. A related metric is the information rate (bit/s), which is defined as the product of the SE and the bandwidth B.

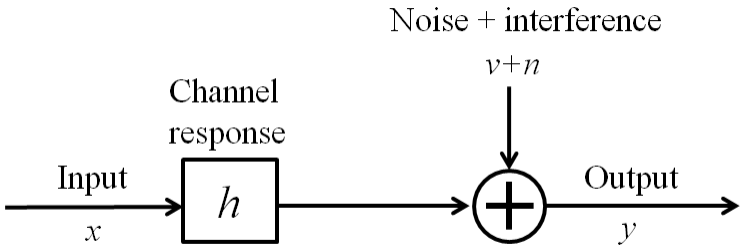

Figure 1.2: A simple discrete memoryless channel with Gaussian noise.

Consider a discrete memoryless channel with input x and ouput y are complex

values as in Figure 1.2. The channel is affected by independent Gaussian noise n and a random interface v can be modeled as

$$y = hx + v + n. \tag{1.2}$$

where $n \sim \mathcal{N}(0, \sigma^2)$ and the channel response $h \in \mathbb{C}$ is known. $\mathbb{E}\{|x|^2\}$ denotes the expectation over time of the power of signal x. Signal power is limited by p, $\mathbb{E}\{|x|^2\} \leq p$ where p is power constraint.

If the channel h is deterministic, and v with zero mean. A known variance $p_v \in \mathbb{R}_+$ is uncorrelated with input x, the channel capacity is bounded as

$$C \geq \log_2 \left(1 + \frac{p|h|^2}{\sigma^2 + p_v}\right). \tag{1.3}$$

Moreover, if the channel h is fading channel, independent of signal and noise. In other words, it is a realization of a random variable $\mathbb{H}$, and $\mathbb{U}$ is a random varible with realization u that affects the interference variance. The ergodic channel capacity is bounded as

$$C \geq \mathbb{E}\left\{ \log_2 \left(1 + \frac{p|h|^2}{\sigma^2 + p_v(h, v)}\right)\right\}, \tag{1.4}$$

where $p_v(h, v) = \mathbb{E}\{|v|^2|h, u\}$ is conditional variance, and the expectation is taken with respect to h, v.

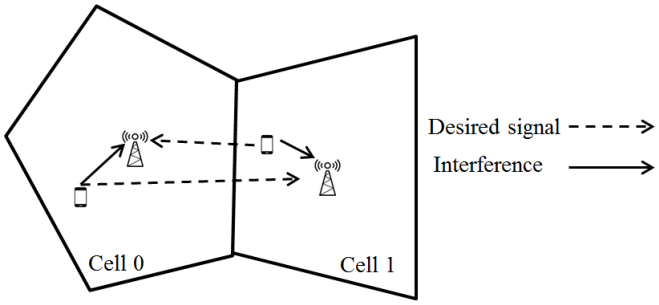

Figure 1.3: A simple cellular system with two cells.

Consider a simple cellular systems as in Figure 1.3, which consists of two cells. Each cell has a single-antenna user and a single-antenna BS. The signal received at BS in cell 0 is

$$y_0 = h_{00}s_0 + h_{10}s_1 + n_0, \tag{1.5}$$

where n_0 is additive noise at BS antenna, h_{ij} is the channel vector from user in cell i to BS in cell j, and s_i is data symbol from user i.

Based on the lower bound of user SE in eq. (1.4), to increase the SE or user capacity, we can increase data power. However, increasing power of a desired user also means increasing the interference to other adjancent cells. Moreover, since receiving antenna is single, then the received signal is scalar. Consequently, we can not distinguish between desired signal and interferenece due to lack of freedom.

With that in mind, the effective way is to increase the number of receiving antennas or in other words, is to obtain the array gain and spatial diversity. Having more receiving antennas helps BS to distinguish between signals (if channel response is

known at BS) by taking the advantage of degree of freedom,and also helps to collect more data power. The received signal now becomes

$$\mathbf{y}_0 = \mathbf{h}_{00}s_0 + \mathbf{h}_{10}s_1 + \mathbf{n}_0. \tag{1.6}$$

By some methods, BSs can estimate the channel and form a suitable receive combining vector $\mathbf{v}_0$ to detect signal as

$$\mathbf{v}_0^H\mathbf{y}_0 = \mathbf{v}_0^H\mathbf{h}_{00}s_0 + \mathbf{v}_0^H\mathbf{h}_{10}s_1 + \mathbf{v}_0^H\mathbf{n}_0. \tag{1.7}$$

Receive combining is a linear projection, which transforms the single-input multiple-output (SIMO) channel into an effective single-input single-output (SISO) channel which can prodive higher SEs than in the single-antenna case, if the combining vector is selected effectively. When number of receiving antenna increase significantly (few hundreads or more), the interfering signal and noise can be canceled out thanks to the law of large number [6].

1.3 Fundamental of massive MIMO

From the existing cellular network architechture as described in the previous section, the Massive MIMO technology from [6], [7] embraces the guideline and design of cellular network, and then makes it more efficent to achieve high SE in the future wireless networks.

Generally, a massive MIMO network is a multicarrier cellular network containing L cells that operate in time division duplex (TDD) protocol. BS in cell j is equipped

with M_j antennas ($M_j >> 1$). BS in cell j simultaneously serves K_j single-antenna UEs on every time/frequency sample, with ratio between number of BS antennas and number of UEs is $\frac{M_j}{K_j} > 1$. Each BS operates independently and exchange signals with its corresponding UEs via linear receive combining and linear transmit precoding. Some main characteristic of massive MIMO are:

- TDD operation: massive MIMO systems prefer to operate in TDD mode. Since with FDD, the channel estimation complexity depends on the number of BS antennas, M which is really huge in case of massive MIMO. By contrast, with TDD, the channel estimation complexity is independent of M. For example, assume that the coherence interval is $T_c = 200$ symbols (corresponding to coherence time of 1 ms and 200 kHz coherence bandwidth). Then, in FDD systems, the number of BS antennas and the number of users are constrained by $M + K < 200$, while the constraint on M and K is $2K < 200$ in case of TDD. With TDD, adding more BS antennas does not affect the resources needed for the channel estimation.

- Linear processing: since the number of users and BS antennas are huge, the signal processing at BSs must deal with large dimensional matrices or vectors. Therefore, simple signal processing is preferable. In massive MIMO, linear processing (linear combing schemes in the uplink and linear precoding schemes in the downlink) is nearly optimal.

- Favorable propagation and channel hardening: these are two most important characteristics, which make channel in massive MIMO system is well-conditioned. More details will be prodived in the next section.

- Since UE is mobile and has limited powered, all complex proccesing and complexity lies in BSs.

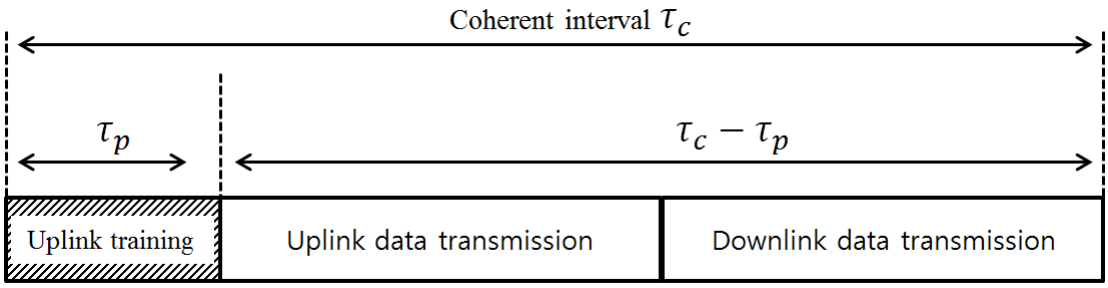

Figure 1.4: Transmission protocol of massive MIMO in TDD mode.

Within a coherence interval, there are three phases: channel estimation, uplink data transmission, and downlink data transmission. A TDD Massive MIMO protocol is shown in Figure 1.5.

To forming receive combining vector for data detection, BSs need to estimate channel to obtain channel statistical information (CSI). This CSI is obtained via the uplink training. All user are assigned a predefined pilot sequence, and they simultaneously sends their pilot sequence to the corresponidng BS in channel estimation phase. The BSs know pilots sequences from all users, and then estimates the channels based the received tranining signals.

1.3.1 Channel model

In massive MIMO systems, we consider channels between UEs and BSs as Rayleigh fading channels. The channel from UE k in cell l to BS in cell j is modeled as

$$\mathbf{h}_{lkj} \sim \mathcal{N}_{\mathbb{C}}(\mathbf{0}_{M_j}, \mathbf{R}_{lkj}), \tag{1.8}$$

where $\mathbf{R}_{lkj}$ is positive semi-definite spatial correlation matrix, and this matrix is assumed to be known at the BS. The spatial correlation matrix describes the macroscopic propagation effects, consisting of antenna gains and radiation patterns at the receiver and transmitter. The trace of this matrix is

$$\beta_{lkj} = \frac{1}{M_j}\mathrm{tr}(\mathbf{R}_{lkj}), \tag{1.9}$$

which determines the average channel gain from one of the antennas at BS in cell j to UE k in cell l. In a special case where there is no correlation between BS antennas, which is called uncorrelated Rayleigh fading channel, we have

$$\mathbf{R}_{lkj} = \beta_{lkj}\mathbf{I}_{M_j}. \tag{1.10}$$

β_{lkj} is commonly called as large-scale fading coefficient, which changes very slowly in time and is usually modeled follwing 3GPP LTE model [8].

1.3.2 Channel hardening and favorable propagation

Channel hardening

With channel hardening property, a fading channel behave as deterministic channel and fading channel can harden to only its mean value (large-scale fading coefficient). This property reduces the need for combating small-scale fading (for example, by adapting the transmit powers). Moreover, if any algorithm in massive MIMO

operates only based on large-scale fading, it does not have to re-run quickly in time since large-scale fading remains unchanged over many coherent intervals. Channel hardening property is presented as

$$\frac{\|\mathbf{h}_{jkj}\|^2}{\mathbb{E}\{\|\mathbf{h}_{jkj}\|^2\}} \to 1 \tag{1.11}$$

almost surely as $M_j \to \infty$.

Favorable propagation

With favorable propagation, the channel vectors of two different users are asymptotically orthogonal. This property makes it easier for the BS to reduce interference between UEs, which generally improves SE and makes linear combining and precoding become sufficient. Favorable propagation is presented as

$$\frac{(\mathbf{h}_{lij})^H \mathbf{h}_{jkj}}{\sqrt{\mathbb{E}\{\|\mathbf{h}_{lij}\|^2\}\mathbb{E}\{\|\mathbf{h}_{jkj}\|^2\}}} \to 0 \tag{1.12}$$

almost surely as $M_j \to \infty$.

1.3.3 System model for uplink and downlink

Channel estimation

As stated before, it is very important for BS in cell j to have the estimated channels from UEs in cell j. Estimated channels from interfering UEs (in adjacent cells) can also be useful to perform interference suppression during data transmission. In channel estimation phase, UE k in cell j transmits its predefined pilot sequence ϕ_{jk} which can have maximum length up to τ_p, which is time slot for channel estimation

in one coherent interval. Pilot sequence is usually assumed to have unit-magnitude elements to remain a constant power level $\|\phi_{jk}\|^2 = \tau_p$. The received training signal at BS in cell j is given by

$$\mathbf{Y}_j^p = \sum_{k=1}^{K_j} \sqrt{p_{jk}} \mathbf{h}_{jkj} \phi_{jk}^H + \sum_{l \neq j}^{L} \sum_{i=1}^{K_l} \sqrt{p_{li}} \mathbf{h}_{lij} \phi_{li}^H + \mathbf{N}_j^p \tag{1.13}$$

where p_{jk} is pilot power coefficient and $\mathbf{N}_j^p \sim \mathcal{N}_{\mathbb{C}}(0, \sigma^2)$ is the independent AWGN noise. $\sum_{k=1}^{K_j} \sqrt{p_{jk}} \mathbf{h}_{jkj} \phi_{jk}^H$ can be regarded as desired pilot signal, which comes from all users in cell j. On the other hand, $\sum_{l \neq j}^{L} \sum_{i=1}^{K_l} \sqrt{p_{li}} \mathbf{h}_{lij} \phi_{li}^H$ is inter-cell interference, which comes from users in other cells.

Using $\mathbf{Y}_j^p$, BS in cell j can estimate channel from its corresponding users, or even from users in other cells. Assume that BS j wants to estimate the channel from UE k, $\mathbf{Y}_j^p$ is multiplied with ϕ_{jk} as

$$\begin{aligned} \mathbf{y}_{jkj}^p &= \mathbf{Y}_j^p \phi_{jk} \\ &= \sqrt{p_{jk}} \mathbf{h}_{jkj} \phi_{jk}^H \phi_{jk} + \sum_{i \neq k}^{K_j} \sqrt{p_{ji}} \mathbf{h}_{jij} \phi_{ji}^H \phi_{jk} + \sum_{l \neq j}^{L} \sum_{i=1}^{K_l} \sqrt{p_{li}} \mathbf{h}_{lij} \phi_{li}^H \phi_{jk} + \mathbf{N}_j^p \phi_{jk}. \end{aligned} \tag{1.14}$$

The final results of intra-cell term and inter-cell term (the second and third terms in (3.5)) depend on the design of pilot sequence. A popular design of pilot sequence is a mutual orthogonal pilot set for one cell and it is reused in other cells.

Finally, BS uses the received pilot signal $\mathbf{y}_{jkj}^p$ to estimate channel by using any estimation technique such as least squared (LS) and minimum mean squared error (MMSE) estimation.

System model for uplink

Each BS detects the desired signals by linear receive combining detector. Assume that UE k in cell j transmits a random data symbol $s_{jk} \sim \mathcal{N}_{\mathbb{C}}(0, p_{kj})$ for $j = 1, ..., L$ and $k = 1, ..., K_j$. p_{kj} is the data power (not instantaneous value but the average energy per sample). The receive combining detector (vector) $\mathbf{v}_{jk} \in \mathbb{C}^{M_j}$ is derived based on the estimated channel $\hat{\mathbf{h}}_{jjk}$. Depending on what kind of linear combining technique is used, $\mathbf{v}_{jk}$ will have different exact form.

The received data signal at BS in cell j is modeled as

$$\begin{aligned}\mathbf{y}_j &= \sum_{l=1}^{L}\sum_{k=1}^{K_l} \mathbf{h}_{lkj} s_{lk} + \mathbf{n}_j \\ &= \sum_{k=1}^{K_j} \mathbf{h}_{jkj} s_{jk} + \sum_{l\neq j}^{L}\sum_{i=1}^{K_l} \mathbf{h}_{lij} s_{li} + \mathbf{n}_j \end{aligned} \tag{1.15}$$

where $\mathbf{n}_j \sim \mathcal{N}_{\mathbb{C}}(\mathbf{0}_{M_j}, \sigma_{UL}^2 \mathbf{I}_{M_j})$ is independent AGWN noise at BS. The first term $\sum_{k=1}^{K_j} \mathbf{h}_{jkj} s_{jk}$ is refered as designed signals, which comes form UEs in cell j, while the second term $\sum_{l\neq j}^{L}\sum_{i=1}^{K_l} \mathbf{h}_{lij} s_{li}$ is interference form UEs in other cells.

The received data signal $\mathbf{y}_j$ is correlated with combining vector corresponding to each desired UE. Assume that BS in cell j wants to detect signal from UE k, the correlation is given as

$$\mathbf{v}_{jk}^H \mathbf{y}_j = \mathbf{v}_{jk}^H \mathbf{h}_{jkj} s_{jk} + \sum_{i\neq k}^{K_j} \mathbf{v}_{jk}^H \mathbf{h}_{jij} s_{ji} + \sum_{l\neq j}^{L}\sum_{i=1}^{K_l} \mathbf{v}_{jk}^H \mathbf{h}_{lij} s_{li} + \mathbf{v}_{jk}^H \mathbf{n}_j. \tag{1.16}$$

The true channel from desired signal $\mathbf{h}_{jkj}$ can be divided into two parts $\mathbf{h}_{jkj} = \hat{\mathbf{h}}_{jkj} + \tilde{\mathbf{h}}_{jkj}$. $\hat{\mathbf{h}}_{jkj}$ is the estimated channels which has relation to the combining vector $\mathbf{v}_{jk}$, and $\tilde{\mathbf{h}}_{jkj}$ is the channel estimation error.

Finally by using the lower bonding technique [9], the signal to interference and noise ratio (SINR) of UE can be calculated and from that, the closed form SINR can also be derived. This closed form is very important so that many algorithms and schemes to increase the performance of massive MIMO networks can be done. If SINR is obtained, it is easy to calculate SE following formula (1.3) or (1.4). Details of calculating SINR and its closed form is given in the next parts.

System model for downlink

Uplink and downlink in massive MIMO system have duality property since the the estimated in uplink is used for percoding in downlink. BS in cell l transmits signal to its corresponding UEs as

$$\mathbf{x}_l = \sum_{i=1}^{K_l} \mathbf{w}_{li} d_{li} \tag{1.17}$$

where $d_{li} \sim \mathcal{N}_{\mathbb{C}}(0, \rho_{li})$ is downlink data signal intended for UE i in cell l and ρ_{li} is the signal power. These signals are assigned to the precoding vector $\mathbf{w}_{li} \in \mathbb{C}^{M_l}$. $\mathbf{w}_{li}$ has relation to the estimated channel $\hat{\mathbf{h}}_{lil}$ from uplink training depending on the purpose of the precoding.

UE k in cell j should receive the signal from its corresponding BS as well as from BS in other cells as

$$y_{jk} = \sum_{l=1}^{L} \sum_{i=1}^{K_l} (\mathbf{h}_{jkl})^H \mathbf{w}_{li} d_{li} + n_{jk}. \tag{1.18}$$

Similar to the model for uplink transmission, the downlink received data y_{jk} can be rewritten as the summation of desired signal, inter-cell and inter-cell interference.

Once again, the lower bonding technique [9] is adapted to calculate the downlink SINR of UE and from that, the closed form SINR in downlink can also be derived.

1.4 Contribution and layout of the thesis

The dissertation consists of seven chapters structured as follows:

In Chapter 1, we sum up all the fundamental knowledge relevant to cellular networks, motivation to massive MIMO networks, and related knowledge such as spectral efficieny, channel estimation technique and system model. Then, we show the outline of the dissertation.

In Chapter 2, we investigate the physical multi-path channel model to propose a pilot assignment algorithmbased on a classic vertex graph coloring algorithm LDO (largest degree ordering) in conjunction with the existing post-processing DFT filter in the channel estimation process. Our idea is to improve the accuracy of the post-processing DFT filter, in other words, the accuracy of the estimated desired channels are improved and so the user's achievable rates are also improved.

In Chapter 3, we propose a disjoint pilot and data power allocation where pilot powers are optimized based on the sum normalized mean squared error (sum NMSE) of channel estimation minimization problem and data powers are optimized based on sum SE maximization problem. The proposed approach combines both indirect and direct methodologies. Specially, pilot power and data power are separately optimized in different optimization problems, and this scheme is able to reduce the complexity.

In Chapter 4, we propose a multiple user-type massive MIMO system and investigate the pilot and data power optimization in the proposed system model. This

idea is motivated by the fact is that in conventional massive MIMO systems, all users belong to the same type. Therefore, we propose a multiple user-type massive MIMO system that consists of two user types: QoS users who are guaranteed to have good and stable QoS, and non-QoS users who are similar to users in conventional systems with no guaranteed QoS. Two optimization problems are proposed and they both are non-convex and very hard to be solved directly. Therefore, we propose two successive convex approximation algorithms to solve these two problems. We also prove that the proposed successive approximation algorithms converge at a local maximum Karush-Kuhn-Tucker (KKT) point.

Finally, in Chapter 5, we give some conclusions on the dissertation and some discussions on the future research directions.

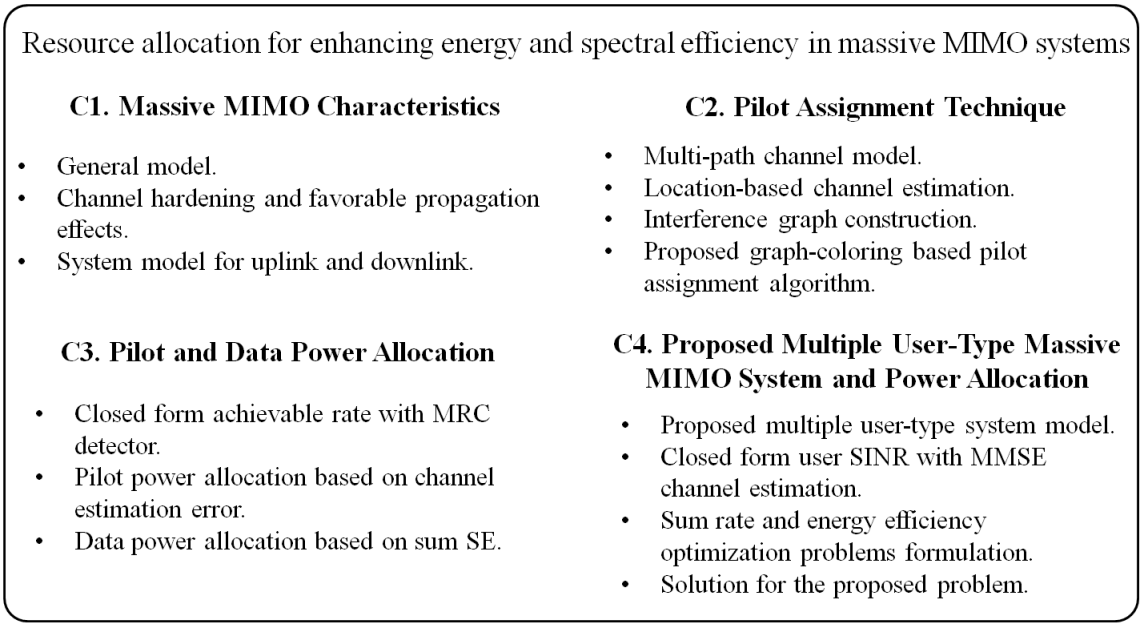

Figure 1.5: Main contributions of this dissertation.

Chapter 2

Pilot assignment with location-based estimation technique

2.1 Introduction and motivation

As briefly dicussed in the Introduction, performance of massive MIMO systems significantly depends on the accuracy of the channel state information estimation process. It has been proved that intra-cell interference and uncorrelated noise can be totally eliminated when the number of BS antennas goes to infinity [10], [11]. However, due to the lack of resources, the same set of orthogonal pilot sequences used in one cell must be reused in other cells, which results in an interference problem known as pilot contamination (PC) since the channel estimation at a BS is contaminated by pilot data sent from other BSs. The inter-cell interference caused by PC will significantly

degrade the capacity of TDD massive MIMO systems [10], [12].

A lot of studies have been conducted to solve the challenging problem of PC [13]-[24]. A multi-cell minimum mean square error (MMSE)-based precoding technique was proposed in [12], where the precoding matrix of each BS was designed to minimize the sum of the squared errors of its own users and the interference with users in other cells. The drawback of this multi-cell MMSE-based precoding technique [13] is its high computational complexity due to large matrix inversion. The time-shifted pilot scheme [14] mitigates PC by dividing the entire system into smaller groups and by using asynchronous transmission among these groups. The time-shifted scheme [14] makes sure that there is no PC among users in different groups when the number of BS antennas goes to infinity, but this leads to the mutual interference between data and pilot sequences in non-asymptotic regime. A smart pilot assignment (SPA) scheme was given in [15] by maximizing the minimum signal-to-interference-plus-noise ratio (SINR) user for each cell in a sequential way, but the convergence cannot be guaranteed. An adaptive pilot allocation (APA) algorithm [16] was proposed by dividing users in the system into two group according to their inter-cell interference when the number of available pilot sequences is larger than number of users in each cell. If the number of available pilot sequences is limited to be equal to the number of users in each cell, then the APA algorithm is the same as random pilot assignment. A PC elimination precoding [17] was proposed by exploiting the property of large-scale fading coefficients of the channel vector between the users and BSs. The precoding [17] can remove PC completely in asymptotic regime, but in non-asymptotic regimes, PC cannot be solved effectively.

The pilot assignment problem in the massive MIMO systems can be interpreted as a vertex graph coloring problem, which is a common mathematical tool and has been used in many fields including allocating network resources [25] [26], where each color is equivalent to a pilot sequence. The goal of vertex graph coloring problem is to color the vertices of a graph with the minimum number of colors, such that no two connected vertices will have the same color. [24] took advantage of the vertex graph coloring problem and applied to the uncorrelated Rayleigh fading channel model in which a channel vector are combined by two components: the small-scale fading vector whose components obey complex Normal distribution with mean 0 and variance 1, and the large-scale fading coefficient which depends on shadow fading and path-loss. Based on that channel model, the authors of [24] showed that when number of BS antennas goes to infinity, the user's SINR only depends on large-scale fading coefficients, from that they proposed a metric to measure the interference between two users only based on large-scale fading. They then created a interference graph by comparing the interference metric value between any two users with a pre-defined threshold, if the interference metric value is larger than the threshold then they consider there is an edge with weight 1 between these two users and if not then there will be no edge, the interference graph is not full-mesh and the potential interference metric between any two users is not fully utilized because the graph only has edges with weight 1. After creating the interference graph, a pilot assignment algorithm GC-PA is proposed based on a classic vertex graph coloring algorithm named Dsatur in which the order of users to be colored are dynamic, which means after each time one user is colored, the algorithm need to find the next selected user to be colored by

calculating the total connection between candidate user and users in adjacent cells who have not been colored. The target of GC-PA is to reduce the mutual interference between users based on large-scale fading so that the total user SINR will be increased. An addition step in [24] is that before running the GC-PA algorithm, [24] has to find the near-optimum threshold by an iterative grid search (IGS).

Inspired by the effectiveness of the post-processing DFT filtering process proposed in [21], in this chapter, we investigate the physical multi-path channel model to propose a pilot assignment algorithmbased on a classic vertex graph coloring algorithm LDO (largest degree ordering) in conjunction with the existing post-processing DFT filter in the channel estimation process. We choose LDO among various classic vertex graph coloring algorithm because of its low complexity, short run-time and the acceptable performance in comparison with other algorithm, the comparing results by running LDO and other various algorithms on different types of graphs are showed in [29]. Our idea aims to improve the accuracy of the post-processing DFT filter, in other words, the accuracy of the estimated desired channels are improved and so the user's achievable rates are also improved. First, a new metric is proposed to measure the potential ICI strength between any two users in different cells based on their AoAs correlation and distances. Next, we construct an ICI graph to depict the potential ICI relationships between every user in the system. Then, taking the inspiration from the classical vertex graph coloring problem, we proposed the vertex graph coloring-based pilot assignment (VGC-PA) algorithm to reduce the ICI among all users in the system by consequently assigning available and suitable pilots to users based on some criteria to ensure connected users with large ICI strength metric will not be assigned

the same pilot sequence. Simulation results of the proposed VGC-PA algorithm using the post-processing DFT filtering process in [21] after the conventional pilot-based channel estimation show significant improvement.

2.2 Channel model

We consider a multi-cell multi-user massive MIMO system composed of L hexagonal cells, where each cell consists of M antennas and K ($K << M$) single-antenna users [6], [10]. In this system model, we consider the typical time-division duplexing (TDD) protocol in massive MIMO systems and we adopt the widely used time block fading model, where the channel vector between the users and BS remains unchanged during the coherence interval [6]. Conventionally, the operation of a massive MIMO system is generally divided into two phases: the channel estimation phase and the data transmission phase.

The multi-path channel model in this chapter is the same as that in [20]. A channel vector $\boldsymbol{h}_{kij}$ with size $M \times 1$ from the k^{th} user in the i^{th} cell to the BS in the j^{th} cell is given as

$$\boldsymbol{h}_{kij} = \frac{1}{\sqrt{P}} \sum_{p=1}^{P} \alpha_{kij}^{p} \boldsymbol{a}(\theta_{kij}^{p}) \sqrt{\beta_{kij}}, \tag{2.1}$$

where P is the number of physical paths and α_{kij}^{p} is the complex gain of the p^{th} physical path with complex Gaussian distribution with zero mean and $E\{|\alpha_{kij}^{p}|^2\} = 1$. The column vector $\boldsymbol{a}(\theta)$ in (3.1) and θ_{kij}^{p} are the steering vector with AoA θ and the AoA of the p^{th} physical path from the k^{th} user in the i^{th} cell to the BS in the j^{th} cell, respectively. β_{kij} in (3.1) is the path-loss and shadow fading coefficient between the

k^{th} user in the i^{th} cell to the BS in the j^{th} cell [20] and can be given as

$$\beta_{kij} = \frac{\alpha}{d_{kij}^{\gamma}}, \tag{2.2}$$

where d_{kij} is the distance between the k^{th} user in the i^{th} cell and the BS in the j^{th} cell, γ is the path-loss exponent, and α depends on the cell edge SNR and cell radius R, given as

$$\alpha[dB] = \text{SNR}^{\text{edge}} + 10\gamma \log(R) + 10 \log(\sigma_n^2), \tag{2.3}$$

where SNR^{edge} is the cell edge SNR in dB and σ_n^2 is the receiver noise power in dB. We assume the value of θ is in $I(0, \pi)$, where $I(s, e)$ is the interval from s to e. When a uniform linear array antennas is used, the steering vector $\boldsymbol{a}(\theta)$ is given as in [21]:

$$\boldsymbol{a}(\theta) = [1, e^{-j2\pi \frac{D}{\lambda} \cos(\theta)}, \cdots, e^{-j2\pi \frac{(M-1)D}{\lambda} \cos(\theta)}]^T, \tag{2.4}$$

where λ is the wavelength of the received signal, $D \leq \frac{\lambda}{2}$ denotes the antenna spacing at the BS antenna array, and T is the transpose operator. In [21], the asymptotic behavior of this multi-path physical model coincides with the conventional flat-fading massive MIMO channel model in [6], [11]. Moreover, in [21], the angle spread of the signal from the user to BS is small when the BS is much higher than the surrounding structure with little scattering, and similar results are shown in [27], [28]. Therefore, we can assume that the AoAs of the multi-path are confined in a small angle interval as $\theta_{kij}^{p} \in I(\theta_{kij}^{\min}, \theta_{kij}^{\max})$ for $1 \leq p \leq P$, where $\theta_{kij}^{\min} = \theta_{kij}^{\text{LOS}} - \delta_\theta$ and $\theta_{kij}^{\max} = \theta_{kij}^{\text{LOS}} + \delta_\theta$ with $\theta_{kij}^{\text{LOS}}$ is the line of sight AoA and δ_θ is the angle spread.

2.2.1 Uplink training phase

In the uplink training phase, the users in all cells transmit their corresponding pilot sequences to their BSs. We assume that the total number of available pilot sequences is S ($S \geq K$), and the pilot group $\boldsymbol{\Phi} = [\boldsymbol{p}_0, \boldsymbol{p}_1, \cdots, \boldsymbol{p}_{S-1}]$ is composed of pilots $\boldsymbol{p}_s$ with length τ that are orthogonal to each other, i.e., $\boldsymbol{\Phi}^H \boldsymbol{\Phi} = \boldsymbol{I}_S$, where $\boldsymbol{I}_S$ is an identity matrix with dimension $S \times S$. The pilot group $\boldsymbol{\Phi}$ is reused in other cells due to limited pilot resources. To explain how one pilot sequence is assigned to the k^{th} user in the i^{th} cell, we define (k, i) as

$$(k, i) \in \{0, 1, \cdots, S-1\}, \tag{2.5}$$

where the set $\{0, 1, \cdots, S-1\}$ denote of all indexes of the pilot sequence set. We consider that all user in one cell have different pilot sequences. Therefore, a set $\{(0, i), (1, i), \cdots, (K-1, i)\}$ has distinct elements and is a subset of $\{0, 1, \cdots, S-1\}$.

In conventional pilot assignment methods, the pilot sequence $\boldsymbol{p}_{(k,i)}$ is randomly assigned to the k^{th} user [6] [11] [14]. The BS in the j^{th} cell receives the pilot sequence $\boldsymbol{Y}_j$ from its users in the cell and also from users in other cells, given as

$$\boldsymbol{Y}_j = \sqrt{\rho_{\mathrm{p}}} \sum_{i=1}^{L} \sum_{k=1}^{K} \boldsymbol{h}_{kij} \boldsymbol{p}_{(k,i)}^H + \boldsymbol{N}_j, \tag{2.6}$$

where ρ_{p} denotes the pilot transmission power and $\boldsymbol{N}_j \in \mathcal{C}^{M \times \tau}$ denotes the additive Gaussian white noise (AWGN) matrix whose entries are independently and identically distributed (i.i.d) Gaussian random variables with zero-mean and variance 1. The estimated value for the channel of the k^{th} user in the j^{th} cell is calculated by correlating

the received pilot sequence $\boldsymbol{Y}_j$ with the pilot sequence $\boldsymbol{p}_{(k,j)}$ as

$$\begin{aligned}\hat{\boldsymbol{h}}_{kjj} &= \frac{1}{\sqrt{\rho_{\mathrm{p}}}}\boldsymbol{Y}_j\boldsymbol{p}_{(k,j)} \\ &= \sum_{i\in\{1,2,\cdots,L\},\boldsymbol{p}_{(k,i)}=\boldsymbol{p}_{(k,j)}} \boldsymbol{h}_{kij} + \boldsymbol{z}_{kj},\end{aligned} \tag{2.7}$$

where $\boldsymbol{z}_{kj} = \frac{1}{\sqrt{\rho_{\mathrm{p}}}}\boldsymbol{N}_j\boldsymbol{p}_{(k,j)}$ denotes the equivalent noise after the correlation process.

2.2.2 Uplink data transmission phase

In the data transmission phase, we consider the uplink data transmission in which users transmit their data signal to their corresponding BS. The received user data signal at the BS in the j^{th} cell can be represented as

$$\boldsymbol{y}_j = \sqrt{\rho_{\mathrm{u}}}\sum_{i=1}^{L}\sum_{k=1}^{K}\boldsymbol{h}_{kij}s_{ki} + \boldsymbol{n}_j, \tag{2.8}$$

where s_{ki} denotes the data symbol from the k^{th} user in the i^{th} cell with $E\{|s_{ki}|^2\} = 1$, ρ_{u} denotes the uplink data transmission power, and $\boldsymbol{n}_j \in \mathcal{C}^{M\times 1}$ denotes the AWGN vector at BS with $E\{\boldsymbol{n}_j\boldsymbol{n}_j^H\} = \boldsymbol{I}_M$. The channel estimation $\hat{\boldsymbol{H}}_{jj} = [\hat{\boldsymbol{h}}_{jj1}, \hat{\boldsymbol{h}}_{jj2}, \cdots, \hat{\boldsymbol{h}}_{jjK}]$ obtained in the uplink training phase is used for the data detection process, and the detected symbol vector for all users in the j^{th} cell is computed as

$$\hat{\boldsymbol{s}}_j = \boldsymbol{D}_j\boldsymbol{y}_j, \tag{2.9}$$

where $\boldsymbol{D}_j \in \mathcal{C}^{K\times M}$ is a detection matrix which is calculated based on $\hat{\boldsymbol{H}}_{jj}$. Among the existing detection algorithms, the matched-filter (MF) detector is considered and so that $\boldsymbol{D}_j = \hat{\boldsymbol{H}}_{jj}^H$.

2.2.3 Location-based channel estimation

To explain the proposed pilot assignment algorithm, the basic idea of location-based channel estimation in [21] is first discussed. Such channel estimation methods are based on a post-processing filtering process at the BS to filter out the interfering channel vector from the users in other cells to the target cell based on the user's geographical location which is calculated using their AoAs with the target cell. The filtering process is done by taking advantage of the following property: $\boldsymbol{a}(\theta)$ can be considered as a single-frequency signal with the frequency $f_{\mathbf{a}} = \frac{D}{\lambda}\cos(\theta)$, so that when the number of the antennas at the BS goes to infinity, the Fourier transform of $\boldsymbol{a}(\theta)$ become a δ-function. The N-points discrete Fourier transform (DFT) $\boldsymbol{A} = [A(0), \cdots, A(N-1)]^T$ of the steering vector $\boldsymbol{a}(\theta)$ is given by

$$X(n) = \sum_{m=0}^{M-1} a(m)e^{-j2\pi nm} = \frac{1 - e^{j2\pi M(\frac{D}{\lambda}\cos(\theta)+\frac{k}{N})}}{1 - e^{j2\pi(\frac{D}{\lambda}\cos(\theta)+\frac{k}{N})}} = \sum_{i=0}^{M-1} e^{-j2\pi i q_n}, \tag{2.10}$$

where $N \geq M$, $0 \leq n \leq N-1$, $a(m) = e^{-j2\pi\frac{mD}{\lambda}\cos(\theta)}$, and $q_n = \frac{D}{\lambda}\cos(\theta) + \frac{n}{N}$. If $e^{-j2\pi i q_n} = 1$ for every $0 \leq i \leq M-1$, then $|A(n)|$ reaches its maximum value M. Let $n^{\lim}$ be

$$n^{\lim} = \arg \max_{0 \leq n \leq N-1} |A(n)|,$$

then

$$n^{\lim} = \lfloor g_N(\theta) \rceil, \tag{2.11}$$

where $\lfloor x \rceil$ is the operation for rounding to the integer closest to x, and the function

$g_N(\theta)$ is given as

$$g_N(\theta) = \begin{cases} N - N\dfrac{D}{\lambda}\cos(\theta), & \theta \in [0,\ \dfrac{\pi}{2}) \\ -N\dfrac{D}{\lambda}\cos(\theta), & \theta \in [\dfrac{\pi}{2}, \pi]. \end{cases} \tag{2.12}$$

Denote the DFT of the estimated channel vector $\hat{\boldsymbol{h}}_{kjj}$ as $\boldsymbol{F}_{kjj} = [F_{kjj}(0), F_{kjj}(1), \cdots, F_{kjj}(N-1)]^T$, and assume that the AoAs of the k^{th} user in the j^{th} cell to its corresponding BS are limited in the interval $[\theta_{kjj}^{\min}\ \theta_{kjj}^{\max}]$. We can use the above property to filter out the DFT value of $\boldsymbol{F}_{kjj}$ outside the interval $I(n_{kjj}^{\min}, n_{kjj}^{\max})$ by setting those outside value to zero. The interval $I(n_{kjj}^{\min}, n_{kjj}^{\max})$ is defined as

$$\begin{aligned} &I(n_{kjj}^{\min}, n_{kjj}^{\max}) \\ &= \begin{cases} [n_{kjj}^{\min}, n_{kjj}^{\max}], & \text{for } n_{kjj}^{\min} \le n_{kjj}^{\max} \\ [0, n_{kjj}^{\max}] \cup [n_{kjj}^{\min}, N-1], & \text{for } n_{kjj}^{\min} > n_{kjj}^{\max}, \end{cases} \end{aligned} \tag{2.13}$$

where $n_{kjj}^{\min}$ and $n_{kjj}^{\max}$ are calculated as

$$\begin{cases} n_{kjj}^{\min} = \lfloor g_N(\theta_{kjj}^{\min}) \rceil \\ n_{kjj}^{\max} = \lfloor g_N(\theta_{kjj}^{\max}) \rceil. \end{cases} \tag{2.14}$$

By using this DFT filtering method, the user signal with its AoAs to the target BS outside the interval $I(\theta_{kjj}^{\min}, \theta_{kjj}^{\max})$ will be filtered out. After the filtering process, we have

$$\hat{F}_{kjj}(n) = \begin{cases} F_{kjj}(n), & n \in I(n_{kjj}^{\min}, n_{kjj}^{\max}) \\ 0 & n \notin I(n_{kjj}^{\min}, n_{kjj}^{\max}). \end{cases} \tag{2.15}$$

Then, the last step is performing the inverse DFT on $\hat{F}_{kjj}(n)$ to get the result $\boldsymbol{f}_{kjj} = [\hat{f}_{kjj}(0), \hat{f}_{kjj}(1), \cdots, \hat{f}_{kjj}(N-1)]^T$. The final estimated channel vector for the k^{th} user in the j^{th} cell to its corresponding BS is $\bar{\boldsymbol{h}}_{kjj} = [\hat{f}_{kjj}(0), \hat{f}_{kjj}(1), \cdots, \hat{f}_{kjj}(M-1)]^T$.

2.3 Pilot assignment algorithm

The key point of the effectiveness of the location-based channel estimation method is based on the non-overlapping AoAs to a target BS of different users with the same pilot. To maximize the performance of this post-processing DFT filtering channel estimation, we need to satisfy the non-overlapping AoAs condition as much as possible, which inspired us to propose the VGC-PA algorithm in this chapter, in contrast to the conventional pilot assignment scheme that assigns pilot randomly and the detail is proposed as following.

2.3.1 Pilot assigment criteria and graph construction

There are two criteria to assign a pilot to users in our proposed systems. The first criteria is to assign the same pilot sequence to users in different cells so that the BSs will have different AoAs from those users, which allows the post-processing DFT filtering of the BS to correctly pass the signal of the desired user and filter out all other users with the same pilot sequence. The second criteria is to assign the same pilot sequence to users when the distances between the desired user and interfere users are sufficiently large. To check these two criteria, we proposed a metric to evaluate the potential ICI between any two users in different cells when the same pilot sequence is assigned to the two users. To measure the ISI between the k^{th} user in the i^{th} cell and the l^{th} user in the j^{th} cell for $i \neq j$, the ICI metric R_{kilj} between them is defined as

$$R_{kilj} = R_{ki\to lj} + R_{lj\to ki} = \frac{|\boldsymbol{\eta}^T(\theta_{kij})\boldsymbol{\eta}(\theta_{ljj})|}{d_{kij}^{\gamma}} + \frac{|\boldsymbol{\eta}^T(\theta_{lji})\boldsymbol{\eta}(\theta_{kii})|}{d_{lji}^{\gamma}} \tag{2.16}$$

where $R_{ki \to lj}$ is the ICI metric that the k^{th} user in the i^{th} cell interferes to target l^{th} user in target j^{th} cell, and θ_{kij} and d_{kij} are the AoA of the signal and distance from the k^{th} user in the i^{th} cell to BS in the j^{th} cell, respectively. γ and $\boldsymbol{\eta}(\theta)$ in (2.16) are path loss exponent and $\boldsymbol{\eta}(\theta) = [\cos(\theta), \sin(\theta)]^T$, respectively. R_{kilj} is used to evaluate the ICI strength between the k^{th} user in the i^{th} cell and the l^{th} user in the j^{th} cell $(i \neq j)$ by considering both the correlation between two AoAs and the distance of the interfering users. A smaller R_{kilj} indicates that the difference in AoA of two users is large and/or the interfering users and target users are far away from each other. Thus, R_{kilj} is a good metric to evaluate the strength of potential ICI between any 2 users if they have the same pilot sequence.

To see the potential ICI relationship between every user in the entire system, we propose an ICI graph where each user corresponds to a vertex and each edge is a connection between one user in a cell and another user in an other cell. One user will have connections to every user the in other cells. The metric over an edge between a vertex corresponding to the k^{th} user in the i^{th} cell and a vertex corresponding to the l^{th} user in the j^{th} cell is R_{kilj} for $i \neq j$. A simple intuitive illustration of an ICI graph is shown in Fig. 2.1 where three cells are considered.

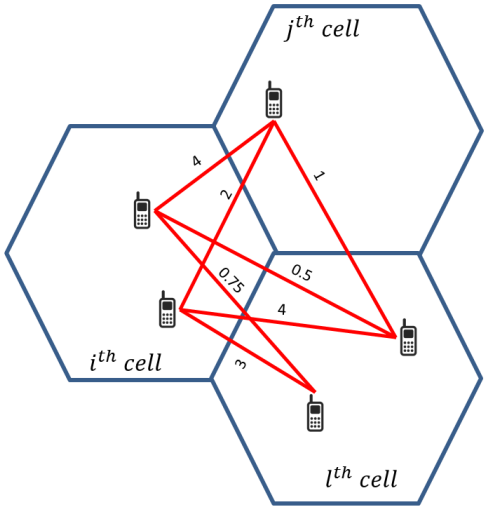

Figure 2.1: An example of construction of an ICI Graph.

2.3.2 Proposed pilot assignment algorithm

To assign pilot sequences efficiently, we consider the vertex graph coloring problem, which has been involved widely in many studies [25] [26]. The goal of vertex graph coloring problem is to color the vertices of a graph with the minimum number of colors, such that no two connected vertices will have the same color. However, there are two major differences between our pilot assignment problem and the conventional vertex graph coloring problem, which can be summarized as follows.

D1) Only S pilot sequences are available

D2) Pilots in one cell have to be orthogonal to each other, which means one pilot can not be reused in one cell.

There are a lot of classic algorithms to color vertices in conventional graph coloring problems, but among them we are inspired by the classical largest degree ordering (LDO) algorithm [29], which sorts vertices in descending order of their degrees and

colors them sequentially with the conventional vertex graph coloring criteria. Let V and E be the sets of all vertices and edges in the graph $G(V, E)$, respectively. The pseudo code of our proposed VGC-PA algorithm is presented in **Algorithm 1**.

Algorithm 1 Proposed VGC-PA Algorithm

Input: System parameters: S, K, L

Output: Pilot assignment for all users in the system

Initialization:

1: Generate ICI graph $G(V, E)$, $\Omega = \varnothing$

2: Calculate $\delta_{(k,i)} = \sum_{(m,j)\in N_{(k,i)}} R_{kimj}$ for all vertices.

3: Sort δ by descending order: $\delta_{(k_0,i_0)} \geq \delta_{(k_1,j_1)} \cdots \geq \delta_{(k_{K*L-1},m_{K*L-1})}$.

4: **for** $l = 0 : 1 : (K * L - 1)$ **do**

5: Find $\Upsilon = \{(k, i_l) | \boldsymbol{p}_{(k,i_l)} \neq \boldsymbol{p}_{(k_l,i_l)}, \text{ for } 0 \leq k \leq K-1\}$

6: Calculate $\varepsilon_s = \sum_{(m,j)\in\Omega, \boldsymbol{p}_{s=(m,j)}} R_{k_l i_l mj}$

7: Assign $\boldsymbol{p}_{(k_l,j_l)} = \boldsymbol{p}_{\arg\min\{\varepsilon_s : s\in\Upsilon\}}$

8: $\Omega = \Omega \cup (k_l, i_l)$

9: **end for**

1. *Initialization (Step 1) and Metric Calculation (Step 2–3)*: For the ICI graph G with vertices set V as the set of all users in the system and edge set E between all users, the metric for every edge is calculated using equation (2.16). After that, the set Ω containing the users that are already assigned pilot sequences is initialized as a null set, i.e $\Omega = \varnothing$. Let (k, i) and $N_{(k,i)}$ be a vertex which corresponds to the k^{th} user in the i^{th} cell and the set of all vertices connected to the (k, i), respectively. Then, the vertex weight $\delta_{(k,i)}$ of the vertex (k, i), is

calculated by summing all of its edge metrics (*Step 2*) and then sorting them in descending order. (*Step 3*).

2. *Condition of Pilot Assignment for users in the same cell (Step 5)*: From the descending ordered value δ in *Step 3*, we generate the available pilot set for the selected user as in *Step 5* since a pilot can not be reused in one cell. $\boldsymbol{p}_{(k,j)}$ in *Step 5* denotes the pilot sequence that is assigned to k^{th} user in the i^{th} cell and (k, i) is defined in (2.5).

3. *Pilot Assignment based on Potential ICI (Step 6–8)*: we define ε_s in *Step 6* to measure the potential ICI strength between users that are already assigned the pilot s in Ω and the selected user in *Step 5* if the selected user is assigned pilot s. Eventually, the pilot with the smallest potential ICI strength ε_s is selected to be assigned to the selected user (k_l, i_l) in *Step 7*. The user (k_l, i_l) will be added to the already assigned user set Ω in *Step 8*.

4. *Looping Condition*: The loop from *Step 5–8* will be terminated when all users in the ordered array in *Step 3* are assigned their corresponding pilots.

2.4 Numerical results

In this section, we evaluate the performance of the proposed VGC-PA algorithm by running the simulations in a multi-cell multi-user massive MIMO system scenario with $L = 7$ hexagonal cells, where each cell has a central BS equipped with M antennas, the number of users in each cell is $K = 12$ and the locations of users are randomly and uniformly distributed around the BS. The simulation system's parameters are

listed in Table 2.1.

Table 2.1: **System parameters**

Number of cells L	7
Number of BS antennas M	$200 \leq M \leq 2000$
Number of users in each cell K	12
Cell radius R	500 m
Transmit power at user $\rho_{\mathrm{u}}(\rho_{\mathrm{p}} = \tau\rho_{\mathrm{u}})$	20 dB
Path loss exponent α	3.5
Cell edge SNR_{edge}	15 dB
Number of physical paths per user P	50
Angle spread δ_θ	10 degrees
Number of orthogonal pilots S	$K \leq S \leq K * L$
Number of DFT points N	8192
Spectral efficiency loss $\mu_S = (S/K)\mu_0$	$\mu_0 = 0.05$

There are two types of distributions of angle spread are considered in the simulation: the first one is the uniform distribution, where the AoAs are uniformly and randomly distributed in the interval $I(\theta^{\mathrm{LOS}} - \delta_\theta, \theta^{\mathrm{LOS}} + \delta_\theta)$ where θ^{LOS} is the light of sight AoA of users and δ_θ is the angle spread, whereas the second one is the Gaussian distribution with mean θ^{LOS} and deviation δ_θ.

We evaluate the performance of our proposed VGC-PA algorithm using two criteria: the mean square error (MSE) and capacity. The MSE of the channel estimation vector is calculated by

$$\mathrm{MSE} = 10\log_{10}\left(\frac{E\{||\bar{\boldsymbol{h}}_{kjj} - \boldsymbol{h}_{kjj}||^2\}}{E\{||\boldsymbol{h}_{kjj}||^2\}}\right)[\mathrm{dB}], \tag{2.17}$$

where $\bar{\boldsymbol{h}}_{kjj}$ is the final DFT filtered estimated channel vector and $\boldsymbol{h}_{kjj}$ is the true channel vector for the k^{th} user in the j^{th} cell.

The capacity of the k^{th} user in the j^{th} cell in uplink data transmission when we adopt an MF detector is calculated as in (2.18) where $\boldsymbol{d}_{kj}^T$ is the k^{th} row vector of MF

$$\mathrm{C}_{kjj} = E\{\log_2(1 + \frac{||\boldsymbol{d}_{kj}^T \boldsymbol{h}_{kjj}||^2}{\sum_{l \neq k} ||\boldsymbol{d}_{kj}^T \boldsymbol{h}_{ljj}||^2 + \sum_{i \neq j} \sum_{m=1}^{K} ||\boldsymbol{d}_{kj}^T \boldsymbol{h}_{mij}||^2 + ||\boldsymbol{d}_{kj}||^2})\} \quad (2.18)$$

detection matrix $\boldsymbol{D}_j$ in equation (2.9).

The proposed VGC-PA algorithm is compared with the following existing solutions: conventional pilot assignment that randomly assigns pilots to the users without any other consideration [6], [11], and the proposed suboptimal pilot assignment algorithm in [21] which is based on the location of sectors in each cells; the proposed algorithm in [21] only focuses on one random target cell.

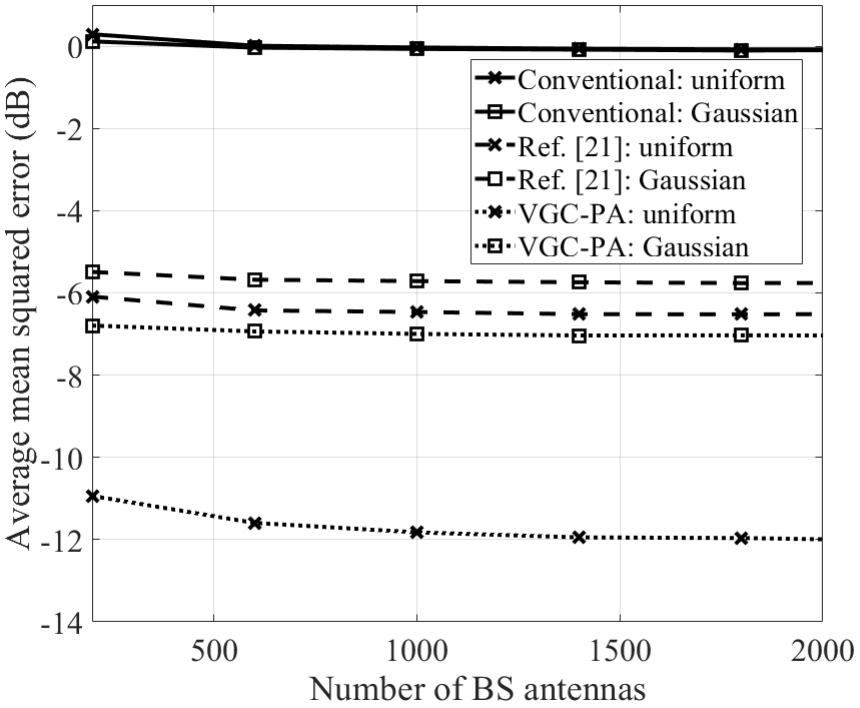

Figure 2.2: Average mean square error comparison when $\boldsymbol{S} = \boldsymbol{K}$ under two different angle spread distributions.

Fig. 2.2 compares the MSE of our proposed VGC-PA algorithm averaged over all channel vectors of all users in the system when the number of available pilots S is equal to the number of users K in each cell, i.e, $S = K$. With the increase of the number of BS antennas, the average MSE of our proposed algorithm significantly outperformed both the suboptimal pilot assignment algorithm in [21] and conventional pilot assignment for a uniform distribution of the angle spread, by about 5 dB compared with proposed algorithm in [21] and 11 dB compared with conventional pilot assignment when $M = 200$. Another notation is that the average MSE of our proposed algorithm continues to reduce gradually with the increase of M while the average MSE of the conventional method hardly reduces and remains bad. However, the proposed VGC-PA algorithm is not as efficient for a Gaussian distribution of the angle spread as for the uniform distribution of angle spread. This is due to the fact that for the the Gaussian distribution of angle spread, the AoAs of the multi-physical paths from users are not confined to an interval. Consequently, some physical paths of target user are filtered out in the post-processing DFT filtering process. If we use the user's actual location information, the proposed algorithm shows better results since the filtering process is more accurate. However, the proposed algorithm is different from the suboptimal pilot assignment algorithm in [21], where the sector's location information in [21] is only effective if each user is distributed evenly in one sector. When one sector has a lot of users and the other sectors have no users, the algorithm in [21] does not work very well.

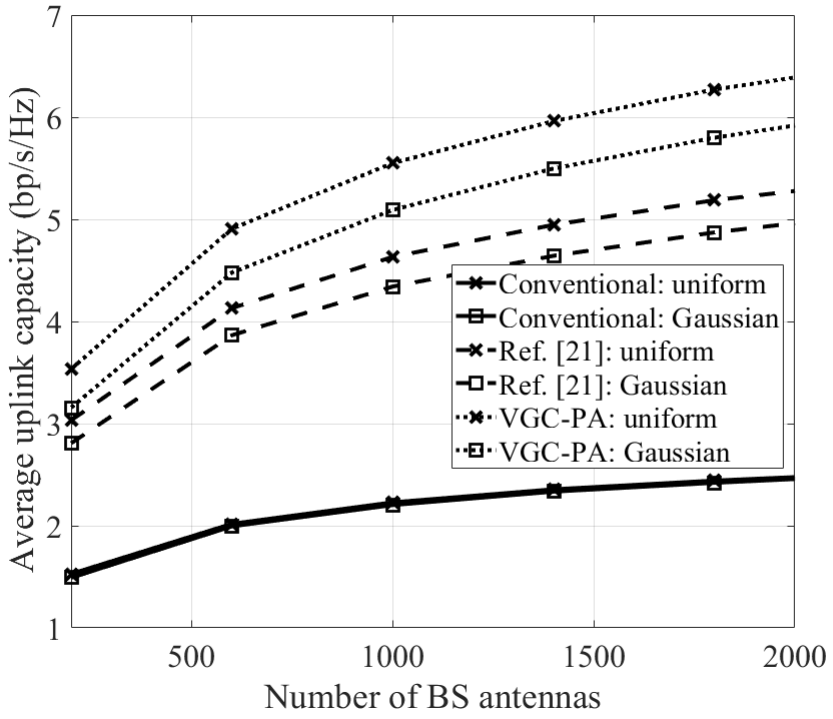

Figure 2.3: Average per user uplink capacity comparison of uplink data transmission when $\boldsymbol{S} = \boldsymbol{K}$ under two different angle spread distributions.

Fig. 2.3 illustrates the simulation results for the user uplink capacity averaged all over the users in the system. In this figure, the uplink capacity of our VGC-PA algorithm is much more improved for both uniform distribution and Gaussian distribution of angle spread when compared to the conventional method and the proposed algorithm in [21]. For a number of BS antennas $M = 200$, the data rate of our proposed algorithm is about 0.4 bp/s/Hz and 2 bp/s/Hz higher than the algorithm in [21] and the conventional method, respectively, for uniform distribution of angle spread. We can also see that the gain of average capacity per user of our VGC-PA algorithm compared with the algorithm in [21] and the conventional method increases quickly when the number of BS antennas increases; this is because with larger M,

the filtering process based on the user's actual location information of our proposed method is significantly more accurate than the asymptotic analysis in [21].

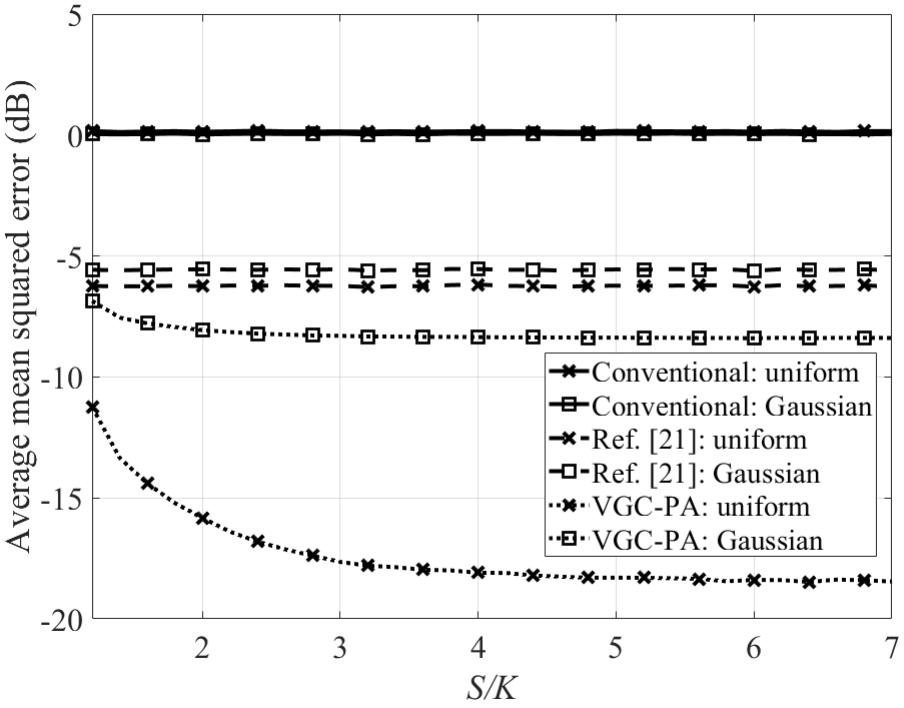

Figure 2.4: Average mean square error comparison against the number of available pilot sequences where the system parameters $\boldsymbol{L = 7}$, $\boldsymbol{K = 12}$ and $\boldsymbol{M = 300}$ are considered.

Fig. 2.4 shows the average MSE against the number of available pilot sequences S, where the system parameters $L = 7, K = 12$ and $M = 300$ are considered. For example, $S/K = 3$ on the x-axis means that the number of available pilot sequences is 36. For both the pilot assignment algorithm in [21] and the conventional pilot assignment, having more pilots, i.e, $S > K$, makes no difference and we can see that in the average MSE curves of those methods, straight lines with zero slope is shown. In contrast, for our proposed method, the average MSE is gradually reduced when

the ratio S/K increase from 1 to nearly 2.5, but when $S/K > 2.5$, the average MSE remains nearly unchanged. This can be explained that with our proposed VGC-PA algorithm, when $1 \leq S/K \leq 2.5$, the more available pilots, the less channel vectors will be interfered by users in other cell with same pilot sequences, which leads to a decrease in the average MSE. However, when $S/K > 2.5$, the accuracy of the filtering processing is good enough to filter out all the remaining interfering users with the same pilot sequence in other cells, and with more pilots available, there is not much improvement in the average MSE.

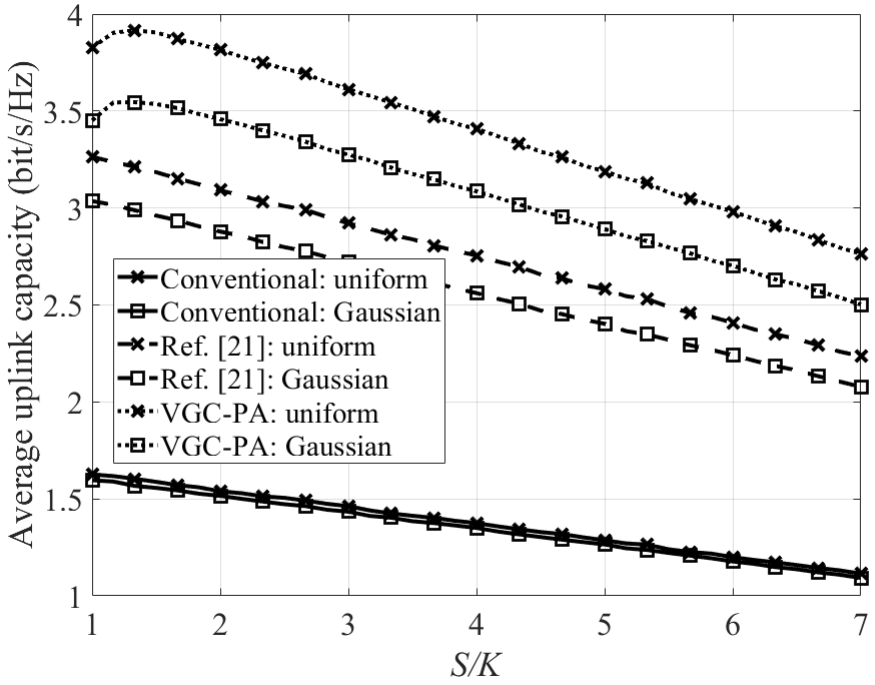

Figure 2.5: Average per user uplink net capacity comparison against the number of available pilot sequences where the system parameters $\boldsymbol{L = 7}$, $\boldsymbol{K = 12}$, $\boldsymbol{M = 300}$, and $\boldsymbol{\mu_0 = 0.05}$ are considered.

Fig. 2.5 illustrates the average per user uplink capacity comparison for uplink data transmission against the number of available pilot sequences where the system

parameters $L = 7, K = 12$ and $M = 300$ are considered. To correctly evaluate the capacity of our proposed algorithm when S/K increases, we need to consider the spectral efficiency loss μ, which is used to calculate the net capacity of system in [6], [11].

$$\mathrm{C}_{kjj}^{\mathrm{net}} = (1 - \mu)\mathrm{C}_{kjj}, \tag{2.19}$$

In the simulation, we set the spectral efficiency loss when $S = K$ as $\mu_0 = 0.05$, and when $S > K$, the corresponding μ_S is calculated as $\mu_S = (S/K)\mu_0$. Similar to the average MSE in fig. 2.4, the net capacity of our proposed algorithm increases when $1 \leq S/K \leq 1.5$ and starts to decrease for $S/K > 1.5$. This phenomenon occurs because when $1 \leq S/K \leq 1.5$, the improvement in MSE results in the improvement in net capacity outperforming the loss of capacity due to the spectral efficiency loss μ_S. However, when $S/K > 1.5$, the improvement in net capacity due to the improvement in MSE can not compensate for the loss of capacity due to the spectral efficiency loss μ_S and consequently, the net capacity decreases rapidly with the increase of ratio S/K.

Chapter 3

Separate pilot power and data power allocation

3.1 Introduction and motivation

To improve the SE of massive MIMO systems, an indirect way is to enhance the channel estimation quality, or in other words, to mitigate the PC problem. For example, a time-shifted pilot scheme [14] divides the system into smaller groups and asynchronously transmit pilot signal and data signals among those groups. The authors of [13] propose a multi-cell minimum mean square error (MMSE)-based precoding which is designed to minimize the sum of the squared errors between its own user signals and other cell user signals. Pilot design is another solution, such as [19] in which the authors use Chu sequences to derive a pilot design criteria to maximize the signal-to-interference-plus-noise ratio (SINR). Pilot assignment is also an interesting solution in which the interference between users is roughly measured based on dif-

ferent types of metrics, and pilot assignment decisions will be made based on these metrics. A smart pilot assignment (SPA) algorithm is proposed in [15] to maximize the minimum user's SINR in each cell of the system sequentially based on only large-scale fading. The authors of [31] try to improve the Quality-of-Service (QoS) of cell edge users by a soft pilot reuse scheme (SPR) in which users in every cell are divided into two group: cell edge users and cell center users, based on a metric calculated from large-scale fading coefficients. After that, SPR assigns to each cell edge user in the system a unique pilot sequence while another orthogonal pilot set is reused for cell center users in every cell. Similar in Chapter 2, the authors of [32] derive a metric to measure the mutual interference between every two users based on their large-scale fading coefficients, and then this metric is used to create an interference graph. Finally, they apply a vertex graph coloring based algorithm to assign pilot sequences to every user in the system. However, different from Chapter 2, [15], [31] and [32] consider uncorrelated fading model. User's statistical information such as the angle-of-arrival (AOA) or spatial covariance matrix can also be used to measure the interference metric and assign pilot sequences when considering correlated fading model such as [22]- [33]. Noticeably, all of the aforementioned works assume equal pilot power and data power for every user, and they also do not focus directly on channel estimation qualities or provide any metric to measure the quality of the channel estimation. In contrast, the authors of [34] focus directly on channel estimation quality by deriving a metric to calculate the relative channel estimation error (RCEE) and its expectation. The authors then use these metrics to propose a pilot power allocation scheme (PPA) to minimize the sum RCEE of users in a target cell under a

total pilot power constraint. To optimize these pilot powers for users in all the cells of the system, they propose a cell-grouping scheme named joint user-cell grouping (JUCG) and apply PPA sequentially to the cell groups. However, while the channel estimation quality is improved, the sum SE of the system is slightly worse than the equal pilot power allocation for every user (EPPA) scheme.

A direct way to improve the SE of massive MIMO systems is to focus directly on the SE formulation to allocate pilot power and data power in an efficient manner. For example, the authors of [35] propose a scheme to maximize the sum SE by allocating the optimal pilot length, pilot power, and data power while total power spent in one coherence interval is fixed; however this scheme considers pilot power and data power for every user to be the same. In [36], an optimized pilot power allocation algorithm is proposed for single-cell massive MIMO systems to maximize the achievable downlink sum rate by using a matched filter. In [37], the authors propose a pilot power allocation scheme to maximize the minimum user SINR in each cell, but the assumption is that all users in each cell use only one pilot sequence, and the pilot sequences for each cell in the system are mutually orthogonal. The authors of [38] consider a single-cell massive MIMO system and investigate the efficiency when applying max-min fairness and max sum SE by deriving closed-form expressions for the user SE containing both pilot power and data power and forming corresponding optimization problems. Interestingly, the authors of [39] considered the maritime massive MIMO system which is quite different with conventional terrestrial cellular massive MIMO system. They proposed a joint optimization of time-shifted pilots and pilot power allocation and claimed that time-shifted approach may be more effective to mitigate

pilot contamination in maritime massive MIMO systems.

In conventional massive MIMO systems, the sum SE is not good since pilot and data power are assigned equally to all users. To maximize sum SE, we normally optimize jointly pilot and data power by forming a sum SE maximization problem with both pilot and data power as the variables. However, pilots are only used for channel estimation so pilot powers should be allocated based on channel estimation quality, not sum SE. Moreover, if channel estimation quality is much more improved, sum SE is also indirectly improved. The PPA schemes in [34] improves channel estimation quality using pilot power allocation but PPA only focuses on one target cell so that the improvement of the channel estimation quality of the system is not significant. Consequently, the sum SE of the system in [34] is not improved. This motivated us to propose a disjoint pilot and data power allocation where pilot powers are optimized based on the sum normalized mean squared error (sum NMSE) of channel estimation minimization problem and data powers are optimized based on sum SE maximization problem. The proposed approach combines both indirect and direct methodologies. Our main contributions in this chapter are as follows.

- We divide the proposed approach into two steps. In the first step, we indirectly improve the sum SE by minimizing the channel estimation error. A closed-form expression for the NMSE of the channel estimation is derived, which only depends on large-scale fading coefficients and pilot powers. We consider two common channel estimation methods: least square (LS) and minimum mean squared error (MMSE). Based on these expressions, we formulate an optimization problem to optimize the sum NMSE of all users in the system with pilot

power as the variables under the constraint of a maximum pilot power per user. The minimization problem for the LS method can be formed as a well-known geometric programming problem and we can use any standard method to find the global optimum point. However it is not as simple for the MMSE method, so we develop an algorithm to find a local optimum point for the sum NMSE minimization problem of the MMSE method. The numerical results show that using only the first step, both channel estimation quality and sum SE can already be improved considerably.

- The second step is to further optimize the sum SE of the system by focusing directly on the SE formulation. We derive a closed-form expression for the user SINR based on a lower bound of user SE, which depends on both pilot and data powers. Pilot power values are taken from the first step and data powers are considered as variables. A maximization problem whose objective function is the sum SE of all users in the system under a maximum data power per user constraint is formed based on the closed-form user SINR however this problem is known as NP-hard so we propose a lower bound on sum SE and form a maximization problem under the same constraint as the original one. An additional advantage of the proposed lower bound optimization problem is that it ensures there is no user getting rejected from service. This second step only focuses on data power and SE expression so it does not affect the channel estimation quality improvement that we achieved in the first step.

3.2 Channel model

We consider a multi-cell multi-user massive MIMO system with L cells, and each cell consists of an M antennas base station (BS) and K ($M >> K$) single-antenna users [6]. The system is assumed to operate in time division duplex (TDD) mode so that the channel in the uplink is reciprocal to the channel in the downlink, and we only need to estimate the channel from the uplink pilot signal. The channel vector $\mathbf{h}_{kj}^{l} \in \mathrm{C}^{M\times 1}$ from the k^{th} user in the j^{th} cell to BS in the l^{th} cell is modeled as follows:

$$\mathbf{h}_{kj}^{l} = \mathbf{g}_{kj}^{l}\sqrt{\beta_{kj}^{l}}, \tag{3.1}$$

where $\mathbf{g}_{kj}^{l} \sim \mathrm{CN}(\mathbf{0}_{M\times 1}, \mathbf{I}_M)$ represents the small-scale fading vector and β_{kj}^{l} denotes the large-scale fading coefficient. This channel model is also called the uncorrelated fading model and every user channel is considered as uncorrelated to the others. Here we assume block fading in which the small-scale fading does not change within one coherence interval, while the large-scale fading changes slowly over time, and thus can be easily tracked at BS and remains unchanged over many coherence intervals.

3.2.1 Uplink training phase

At the beginning of every coherence interval, user channels need to be acquired at BSs first, and from that BSs can create precodings or detectors for uplink or downlink signal transmission. BSs acquire user channels by estimating them from the uplink pilot signals. We assume that each coherence interval has length τ_c with τ_p used for the uplink pilot signal, and the remaining $\tau_c - \tau_p$ is for uplink data transmission [32], [34], [35], [38]. Since in this chapter, we only focus on the uplink

so we assume that all the remaining in one coherence time $\tau_c - \tau_p$ is used for uplink data transmission to make notations simple without loss of generality. We further assume that users within one cell are assigned mutual orthogonal pilot sequences and this pilot set is reused in every other cells. The K orthogonal pilots set is denoted as

$$\mathbf{\Phi} = [\phi_1, \phi_2, \ldots, \phi_K]^T \in C^{K \times \tau_p}, \tag{3.2}$$

$$\phi_i^H \phi_i = \tau_p, \phi_i^H \phi_j = 0, \forall i \neq j. \tag{3.3}$$

Hence, the pilot signal received at the BS in the j^{th} cell is

$$\mathbf{Y}_j = \sum_{i=1}^{L} \sum_{n=1}^{K} \sqrt{\rho_{ni}} \mathbf{h}_{ni}^j \phi_n^H + \mathbf{N}_j, \tag{3.4}$$

where ρ_{ni} is the pilot power of the n^{th} user in the i^{th} cell, and $\mathbf{N}_j \in C^{M \times \tau_p}$ represents the additive white Gaussian noise at the BS in the j^{th} cell with independent and identically distributed zero-mean and unit-variance elements.

To estimate the channel between the BS in the j^{th} cell and the k^{th} user in the j^{th} cell, the received pilot signal in (3.4) is correlated with the k^{th} pilot

$$\mathbf{y}_{kj} = \mathbf{Y}_j \phi_k = \tau_p \sqrt{\rho_{kj}} \mathbf{h}_{kj}^j + \sum_{i \neq j}^{L} \tau_p \sqrt{\rho_{ki}} \mathbf{h}_{ki}^j + \mathbf{n}_{kj}, \tag{3.5}$$

where $\mathbf{n}_{kj} = \mathbf{N}_j \phi_k$ denotes the equivalent noise after the correlation process and whose elements also follow complex Gaussian distributions with zero-mean.

$$\hat{\mathbf{h}}_{kj}^{j,\text{LS}} = \frac{1}{\tau_p \sqrt{\rho_{kj}}} \mathbf{y}_{kj}. \tag{3.6}$$

With the MMSE method [41], the estimated channel is calculated as

$$\hat{\mathbf{h}}_{kj}^{j,\text{MMSE}} = \frac{\sqrt{\rho_{kj}} \beta_{kj}^j}{\sum_{i=1}^{L} \tau_p \rho_{ki} \beta_{ki}^j + 1} \mathbf{y}_{kj}. \tag{3.7}$$

3.2.2 Uplink achievable rate with MRC detector

After obtaining estimated channels, BSs create detectors from the estimated channels to estimate data signals from its own users. In this chapter, we consider a simple linear detector: maximum ratio combining (MRC). The data signal of the k^{th} user in the j^{th} cell detected by MRC at the BS in the j^{th} cell is given as

$$\begin{aligned}\hat{s}_{kj} &= (\hat{\mathbf{h}}_{kj}^{j,\diamond})^H \left(\sum_{l=1}^{L} \sum_{n=1}^{K} \sqrt{p_{nl}} \mathbf{h}_{nl}^{j} s_{nl} + \mathbf{z}_j \right) \\ &= \sqrt{p_{kj}} (\hat{\mathbf{h}}_{kj}^{j,\diamond})^H \mathbf{h}_{kj}^{j} s_{kj} + \sum_{l=1}^{L} \sum_{n \neq k}^{K} \sqrt{p_{nl}} (\hat{\mathbf{h}}_{kj}^{j,\diamond})^H \mathbf{h}_{nl}^{j} s_{nl} + (\hat{\mathbf{h}}_{kj}^{j,\diamond})^H \mathbf{z}_j, \end{aligned} \tag{3.8}$$

where $s_{nl} \sim CN(0,1)$ is the transmitted signal from the n^{th} user in the l^{th} cell , p_{nl} is the data power corresponding to the signal s_{nl}, $\mathbf{z}_j$ is additive white Gaussian noise at the BS in the j^{th} cell and $\hat{\mathbf{h}}_{kj}^{j,\diamond} (\diamond = \{\text{LS}, \text{MMSE}\})$ is the MRC detection vector. Using the lower bounding technique on user SE as in [9, Eq.(12)], the effective SINR for the k^{th} user in the j^{th} cell is given in (3.9) below

$$\text{SINR}_{kj} = \frac{p_{kj} |\mathbf{E}\{(\hat{\mathbf{h}}_{kj}^{j,\diamond})^H \mathbf{h}_{kj}^{j}\}|^2}{\sum_{l=1}^{L} \sum_{n}^{K} p_{nl} \mathbf{E}\{|(\hat{\mathbf{h}}_{kj}^{j,\diamond})^H \mathbf{h}_{nl}^{j}|^2\} - p_{kj} |\mathbf{E}\{(\hat{\mathbf{h}}_{kj}^{j,\diamond})^H \mathbf{h}_{kj}^{j}\}|^2 + \mathbf{E}\{\|\hat{\mathbf{h}}_{kj}^{j,\diamond}\|^2\}} \tag{3.9}$$

Remark 1: The closed-form expression for SINR_{kj} is the same for both LS and MMSE methods and is given in (3.10). The closed-form (3.10) can be easily obtained from [34, *Theorem 1*] by using unequal data power allocation in the Theorem.

$$\text{SINR}_{kj} = \frac{M \rho_{kj} p_{kj} \tau_p (\beta_{kj}^{j})^2}{\left(\sum_{l=1}^{L} \rho_{kl} \tau_p \beta_{kl}^{j} + 1 \right) \left(\sum_{l=1}^{L} \sum_{n=1}^{K} p_{nl} \beta_{nl}^{j} + 1 \right) + \sum_{l \neq j}^{L} M \rho_{kl} p_{kl} \tau_p (\beta_{kl}^{j})^2}. \tag{3.10}$$

We can see that both pilot and data power are presented in the closed-form SINR as in (3.10), so the common way to optimize the sum SE is forming a maximization

problem based on this closed form using pilot power and data power as the variables. We will describe this joint optimization in the next part to compare with our disjoint pilot and data power optimization approach.

3.3 Separate pilot power and data power allocation scheme

To achieve high SE, we need to detect signals with high accuracy, or in other words, the quality of channel estimation needs to be high. This means if we want to improve the SE of the system, the first thing we need to do is to improve the channel estimation quality. Motivated by [34], we also focus directly on channel estimation error and try to mitigate it. To do that, we use a common metric, normalized mean square error (NMSE) [20] [42], to measure the channel estimation error between the true channel and estimated channel. The NMSE of the k^{th} user in the j^{th} cell is given as

$$\eta_{kj}^{\diamond} = \frac{\mathbf{E}\{\|\mathbf{h}_{kj}^{j} - \hat{\mathbf{h}}_{kj}^{j,\diamond}\|^2\}}{\mathbf{E}\{\|\mathbf{h}_{kj}^{j}\|^2\}}, \tag{3.11}$$

where $\diamond$ denotes the LS or MMSE estimation method. The expectation in (3.11) is taken over many coherence intervals in which the small-scale fading changes after each interval while the large-scale fading remains unchanged.

Theorem 1: The closed-form expression of NMSE for LS and MMSE methods are given as follows.

$$\eta_{kj}^{\text{LS}} = \frac{\sum_{i \neq j}^{L} \tau_p \rho_{ki} \beta_{ki}^{j} + 1}{\tau_p \rho_{kj} \beta_{kj}^{j}} \tag{3.12}$$

$$\eta_{kj}^{\text{MMSE}} = \frac{\sum_{i \neq j}^{L} \tau_p \rho_{ki} \beta_{ki}^{j} + 1}{\sum_{i=1}^{L} \tau_p \rho_{ki} \beta_{ki}^{j} + 1} \tag{3.13}$$

Proof: We first calculate the closed-form expression of NMSE for the LS method. From (3.5) and (3.6), the numerator of (3.11) for LS is calculated as

$$\mathbf{E}\{\|\mathbf{h}_{kj}^{j} - \hat{\mathbf{h}}_{kj}^{j,\text{LS}}\|^2\} = M \frac{\sum_{i \neq j}^{L} \tau_p \rho_{ki} \beta_{ki}^{j} + 1}{\tau_p \rho_{kj}}. \tag{3.14}$$

The denominator of (3.11) is given as

$$\mathbf{E}\{\|\mathbf{h}_{kj}^{j}\|^2\} = M \beta_{kj}^{j}. \tag{3.15}$$

From (3.14) and (3.15), we have the closed form of NMSE for the LS method as in (3.12).

We now calculate the closed form of NMSE for MMSE method. The channel estimation error $\tilde{\mathbf{h}}_{kj}^{j,\text{MMSE}} = \mathbf{h}_{kj}^{j,\text{MMSE}} - \hat{\mathbf{h}}_{kj}^{j,\text{MMSE}}$ is distributed as

$$\tilde{\mathbf{h}}_{kj}^{j,\text{MMSE}} \sim CN\left(\mathbf{0}, \beta_{kj}^{j} - \frac{\tau_p \rho_{kj} (\beta_{kj}^{j})^2}{\sum_{i=1}^{L} \rho_{ki} \tau_p \beta_{ki}^{j} + 1} \mathbf{I}_M\right). \tag{3.16}$$

Using (3.16), the numerator of (3.11) for MMSE is calculated as

$$\begin{aligned} \mathbf{E}\{\|\mathbf{h}_{kj}^{j} - \hat{\mathbf{h}}_{kj}^{j,\text{MMSE}}\|^2\} &= \mathbf{E}\{\|\tilde{\mathbf{h}}_{kj}^{j,\text{MMSE}}\|^2\}. \\ &= M \frac{\beta_{kj}^{j} (\sum_{i \neq j}^{L} \rho_{ki} \tau_p \beta_{ki}^{j} + 1)}{\sum_{i=1}^{L} \rho_{ki} \tau_p \beta_{ki}^{j} + 1}. \end{aligned} \tag{3.17}$$

Finally, from (3.15) and (3.17), we have the closed form of NMSE for MMSE method as in (3.13).

This NMSE closed form will be used to form an optimization problem to minimize the sum NMSE of all users in the system. After improving the channel estimation quality, we will focus directly on sum SE by forming a maximization problem using the closed form SINR in (3.10). The details are as follows.

3.3.1 Indirecly improve sum SE

We can see that the closed forms for both NMSE and SINR only depend on large-scale fading coefficients ,which change very slowly in time comparing to small-scale fading, meaning that a power allocation algorithm is suitable for massive MIMO and is easier to apply than in conventional MIMO, where the effect of small-scale fading is dominant.

LS channel estimation

We now formulate the following optimization problem to minimize the sum of estimation errors of all users in the system using the LS method

$$\begin{aligned} \underset{\{\rho_{kj}\}}{\text{minimize}} \quad & \sum_{j=1}^{L}\sum_{k=1}^{K} \eta_{kj}^{\text{LS}} \\ \text{subject to} \quad & 0 \leq \rho_{kj} \leq \rho_{kj}^{\max}, \forall k, j, \end{aligned} \tag{3.18}$$

where $\rho_{kj}^{\max}$ is the maximum pilot power that the k^{th} user in the j^{th} cell can use for a pilot symbol.

From the closed form of η_{kj}^{LS} in (3.12), this problem is non-convex. Fortunately, since all variables $\rho_{kj}, \forall k, j$ are non-negative, the numerator of η_{kj}^{LS} is a posynomial function and the denominator is a monomial function so consequently, the objective function $\sum_{j=1}^{L}\sum_{k=1}^{K} \eta_{kj}^{\text{LS}}$ is a posynomial function, and it is in the form of a geometric program (GP) [43]. GP can be reformulated to a convex optimization problem by changing its variables to log domain, so with GP, we can find the global optimal solution. GP can be efficiently solved by many GP solvers such as SeduMi [44], SDPT3 [45], and MOSEK [46]. Here we choose the MOSEK solver and to simplify its implementation in Matlab, we use the high-level modeling frameworks CVX [47].

MMSE channel estimation

Similar to LS method, the optimization problem for the MMSE method is given below

$$\begin{aligned} \underset{\{\rho_{kj}\}}{\text{minimize}} \quad & \sum_{j=1}^{L}\sum_{k=1}^{K} \eta_{kj}^{\text{MMSE}} \\ \text{subject to} \quad & 0 \leq \rho_{kj} \leq \rho_{kj}^{\max}, \forall k, j, \end{aligned} \tag{3.19}$$

However, the closed form of η_{kj}^{MMSE} in (3.13) is not a posynomial function so generally, problem (3.19) is not in GP form, therefore, we seek a local optimum solution. First, we reformulate (3.13) to its epigraph form as

$$\begin{aligned} \underset{\{\rho_{kj}\}}{\text{minimize}} \quad & \sum_{j=1}^{L}\sum_{k=1}^{K} c_{kj} \\ \text{subject to} \quad & 0 \leq \rho_{kj} \leq \rho_{kj}^{\max}, \forall k, j \\ & \eta_{kj}^{\text{MMSE}} \leq c_{kj}, \forall k, j. \end{aligned} \tag{3.20}$$

The only non-posynomial in (3.20) lies in the closed form of η_{kj}^{MMSE}, which we now approximate by a monomial function via the following lemma.

Lemma 1. [49, *Lemma 1*]: Consider a posynomial function with variables vector $\mathbf{x}$

$$g(\mathbf{x}) = \sum_{i} u_i(\mathbf{x}), \tag{3.21}$$

where $u_i(\mathbf{x})$ is monomial function. Then we have the lower bound

$$g(\mathbf{x}) \geq \tilde{g}(\mathbf{x}) = \prod_{i} \left(\frac{u_i(\mathbf{x})}{\alpha_i} \right)^{\alpha_i}, \tag{3.22}$$

where α_i is the non-negative coefficient corresponding to $u_i(\mathbf{x})$. Moreover, if

$$\alpha_i = \frac{u_i(\mathbf{x_0})}{g(\mathbf{x_0})}, \forall i, \tag{3.23}$$

where x_0 is a fixed non-negative point, then $\tilde{g}(\mathbf{x_0})$ is the best local monomial approximation to $g(\mathbf{x_0})$ near x_0 in the sense of a first-order Taylor approximation.

Using *Lemma 1*, the denominator of η_{kj}^{MMSE} can be approximated as

$$\sum_{i=1}^{L} \tau_p \rho_{ki} \beta_{ki}^{j} + 1 \geq \alpha_{k0} \prod_{i}^{L} \left(\frac{\tau_p \rho_{ki} \beta_{ki}^{j}}{\alpha_{ki}} \right)^{\alpha_{ki}}, \tag{3.24}$$

where α_{k0} is the coefficient corresponding to the element 1, and the other α_{ki} correspond to $\tau_p \rho_{ki} \beta_{ki}^{j}$. Eventually, the upper bound approximation $\tilde{\eta}_{kj}^{\text{MMSE}}$ of η_{kj}^{MMSE} is given as

$$\eta_{kj}^{\text{MMSE}} \leq \tilde{\eta}_{kj}^{\text{MMSE}} = \frac{\sum_{i \neq j}^{L} \tau_p \rho_{ki} \beta_{ki}^{j} + 1}{\alpha_{k0} \prod_{i}^{L} \left(\frac{\tau_p \rho_{ki} \beta_{ki}^{j}}{\alpha_{ki}} \right)^{\alpha_{ki}}}, \forall k, j \tag{3.25}$$

The optimization problem (3.20) now is approximated by the GP

$$\begin{aligned} \underset{\{\rho_{kj}\}}{\text{minimize}} \quad & \sum_{j=1}^{L} \sum_{k=1}^{K} c_{kj} \\ \text{subject to} \quad & 0 \leq \rho_{kj} \leq \rho_{kj}^{\max}, \forall k, j \\ & \tilde{\eta}_{kj}^{\text{MMSE}} \leq c_{kj}, \forall k, j, \end{aligned} \tag{3.26}$$

Theorem 2: By adapting the general inner approximation algorithm for non-convex optimization problems [48] to solve problem (3.20), we will iteratively solve the approximated GP (3.26) and update the coefficients α_{k0}, α_{kj} after each iteration from the optimized pilot power values obtained in the previous iteration. The solution is going to converge to a local minimum Karush-Kuhn-Tucker (KKT) point of (3.20). Details are given in **Algorithm 1**.

Proof: The approximation technique in [48] approximates a non-convex problem by a convex one, and GP can also be reformulated to convex problems so that we can apply this technique to solve our non-GP problem (3.20). The key issue is that

we need to approximate the non-posynomial constraint by a posynomial constraint which needs to satisfy the following three conditions:

- $f(\mathbf{x}) \leq \tilde{f}(\mathbf{x})$ for all feasible $\mathbf{x}$,
- $f(\mathbf{x}_0) = \tilde{f}(\mathbf{x}_0)$, $\mathbf{x}_0$ is the optimal point of the approximated problem from previous iteration
- $\nabla f(\mathbf{x}_0) = \nabla \tilde{f}(\mathbf{x}_0)$,

where $f(\mathbf{x})$ is the original non-psynomial constraint function and $\tilde{f}(\mathbf{x})$ is the approximated one. $\tilde{\eta}_{kj}^{\mathrm{MMSE}}$ in (3.25) satisfies the first and second conditions because of Lemma 1, while the last condition is easily verified by taking the derivatives of η_{kj}^{MMSE} and $\tilde{\eta}_{kj}^{\mathrm{MMSE}}$. The first condition ensures that any optimal point of the approximation problem (3.26) is a feasible point of the original problem (3.20), so that if the optimal point from the previous iteration is not a solution for current iteration, the objective function is guaranteed to decrease. The second and last conditions guarantee that the KKT condition will be satisfied when the iteration process converges. The detailed proof of KKT point convergence is well presented in [48], so we do not to present it here.

Algorithm 2 Iterative GP Approximation Algorithm for Solving (3.20)

Input: Predefine maximum pilot power $\rho_{kj}^{\max}$ and select an feasible initial values for $\rho_{kj}, \forall k, j$, set the iteration counter $i = 1$.

do

1. $i = i + 1$.
2. Update α_{k0}, α_{kj} using (3.23) and pilot power values from previous i^{th} iteration: $\rho_{kj}, \forall k, j$.
3. Solve the approximated GP (3.26) to get the optimal pilot power set: $\rho_{kj}^{\text{opt}}, \forall k, j$.
4. Update values for pilot power at $(i+1)^{\text{th}}$ iteration: $\rho_{kj} = \rho_{kj}^{\text{opt}}, \forall k, j$.

While (not converge)

Output: The local optimum solution $\rho_{kj}, \forall k, j$.

Particularly, **Algorithm 1** first predefines the maximum pilot power for all users in the system and chooses arbitrary initial values for the optimized set $\rho_{kj}, \forall k, j$ which has to be feasible. After that, in each iteration, the values of the coefficients $\alpha_{k0}, \alpha_{kj}, \forall k, j$ are updated as in (3.23) by using the optimized pilot power set from previous iteration. The non-posynomial constraints $\eta_{kj}^{\text{MMSE}}, \forall k, j$ are approximated by the posynomial constraints $\tilde{\eta}_{kj}^{\text{MMSE}}$ as in (3.25) using the coefficients we just calculated. Finally, the approximated GP (3.26) is solved to obtain the optimized pilot power set corresponding to this iteration. This procedure is repeated until it converges to a local optimal KKT point. The convergence condition can be set as the

difference in objective values between two consecutive iterations being smaller than a given threshold or when the iteration counter reaches a particular number (actually, **Algorithm 1** converges quite fast, normally after 15 iterations, with the difference in objective values between two consecutive iterations being smaller than 0.01%).

3.3.2 Directly improve sum SE

After improving the channel estimation, we now focus directly on allocating data power to maximize the sum SE of the system. Using the closed-from expression of user SINR in (3.10), we formulate an optimization problem to maximize the sum SE of the system as

$$\begin{aligned} \underset{\{p_{kj}\}}{\text{maximize}} \quad & \frac{\tau_c - \tau_p}{\tau_c} \sum_{j=1}^{L} \sum_{k=1}^{K} \log_2(1 + \text{SINR}_{kj}) \\ \text{subject to} \quad & 0 \leq p_{kj} \leq p_{kj}^{\max}, \forall k, j, \end{aligned} \tag{3.27}$$

where $p_{kj}^{\max}$ is the maximum data power that the k^{th} user in the j^{th} cell can use for a data symbol; notice that the only variables here are data powers $p_{kj}, \forall k, j$, since the values of pilot power $\rho_{kj}, \forall k, j$ are taken from the previous enhancing channel estimation quality step.

It is proved that the problem of sum rate maximization by power allocation with the presence of interference is an NP-hard problem, even under perfect CSI [50]. So that, we propose a lower bound on the sum SE, which is given as

$$\sum_{j=1}^{L} \sum_{k=1}^{K} \log_2(1 + \text{SINR}_{kj}) \geq \sum_{j=1}^{L} \sum_{k=1}^{K} \log_2(\text{SINR}_{kj}) = \log_2 \left(\prod_{j=1}^{L} \prod_{k=1}^{K} \text{SINR}_{kj} \right). \tag{3.28}$$

The proposed lower bound belongs to the geometric mean optimization class, which never produces zero power solution. So that this lower bound optimization guarantees

that every users in the system gets non-zero data power or in other words, no users are rejected from service. Finally, we obtain the maximization problem for lower bound on the sum SE as

$$\begin{aligned} \underset{\{p_{kj}\}}{\text{maximize}} \quad & \prod_{j=1}^{L}\prod_{k=1}^{K} \text{SINR}_{kj} \\ \text{subject to} \quad & 0 \leq p_{kj} \leq p_{kj}^{\max}, \forall k, j. \end{aligned} \tag{3.29}$$

This problem is again, a geometric program and it can be solved efficiently by any GP solver.

3.3.3 Joint pilot-data power allocation

Normally, having the closed-form expression of SINR (3.10) with pilot and data power as the variables, we can immediately form a joint pilot-data power allocation for sum SE maximization problem as follows:

$$\begin{aligned} \underset{\{p_{kj},\rho_{kj}\}}{\text{maximize}} \quad & \frac{\tau_c - \tau_p}{\tau_c} \sum_{j=1}^{L}\sum_{k=1}^{K} \log_2(1 + \text{SINR}_{kj}) \\ \text{subject to} \quad & 0 \leq p_{kj} \leq p_{kj}^{\max}, \forall k, j, \\ & 0 \leq \rho_{kj} \leq \rho_{kj}^{\max}, \forall k, j. \end{aligned} \tag{3.30}$$

This problem is also NP-hard [50]. Similar to (3.29), we maximize the lower bound of sum SE instead

$$\begin{aligned} \underset{\{p_{kj},\rho_{kj}\}}{\text{maximize}} \quad & \prod_{j=1}^{L}\prod_{k=1}^{K} \text{SINR}_{kj} \\ \text{subject to} \quad & 0 \leq p_{kj} \leq p_{kj}^{\max}, \forall k, j, \\ & 0 \leq \rho_{kj} \leq \rho_{kj}^{\max}, \forall k, j. \end{aligned} \tag{3.31}$$

Once again, this is a geometric program optimization problem similar to GP (3.29) but both pilot and data powers are considered as variables in one sum SE maximization problem.

3.4 Numerical results

In this section, we present the simulation results to show the advantages of our proposed approach. We consider a massive MIMO system with four square cells using wrap-around topology [40] to cover a 500 m^2 area. Wrap-around topology is commonly used in evaluating the performance of power allocation in massive MIMO systems since it helps to even out the interference of every cell, so that it is fair to all cells in evaluating the effectiveness of the proposed power allocation scheme. At the center of each cell is a BS simultaneously serving $K = 8$ users. These K users are uniformly distributed in the cell, where the distance is not smaller than 35 m from the BS. The pilot length is fixed $\tau_p = K$ [35], [38]. The system bandwidth and noise variance are 20 MHz and -94 dBm, respectively. The large-scale fading coefficient is calculated using the 3GPP LTE model [8]

$$\beta_{ki}^{j} = -35.3 - \gamma \log_{10}(d_{ki}^{j}) + z_{ki}^{j}, \tag{3.32}$$

where -35.3 is the average channel gain in dB at a reference distance of 1m, $\gamma = 3.76$ denotes the path-loss exponent, d_{ki}^{j} is the distance in meters from the k^{th} user in the i^{th} cell to the BS in the j^{th} cell, and z_{ki}^{j} represents the shadow fading, which has a log-normal distribution with a standard deviation of 5 dB. The maximum pilot and data powers for every user are the same and $p_{kj}^{\max} = \rho_{kj}^{\max} = 300$ mW, $\forall k, j$.

3.4.1 Channel estimation quality evaluation

In this subsection, we would like to compare the channel estimation quality of our proposed approach, named disjoint pilot-data power allocation (DPDPA) with the equal pilot power allocation (EPPA) scheme, PPA scheme [34], and joint pilot-data power allocation (JPDPA) scheme, which is previously described in previous part in this chapter. For fairness in comparison with PPA scheme in [34], the total pilot power budget of the users in each cell for PPA is set to $P = K\rho_{kj}^{\max}$.

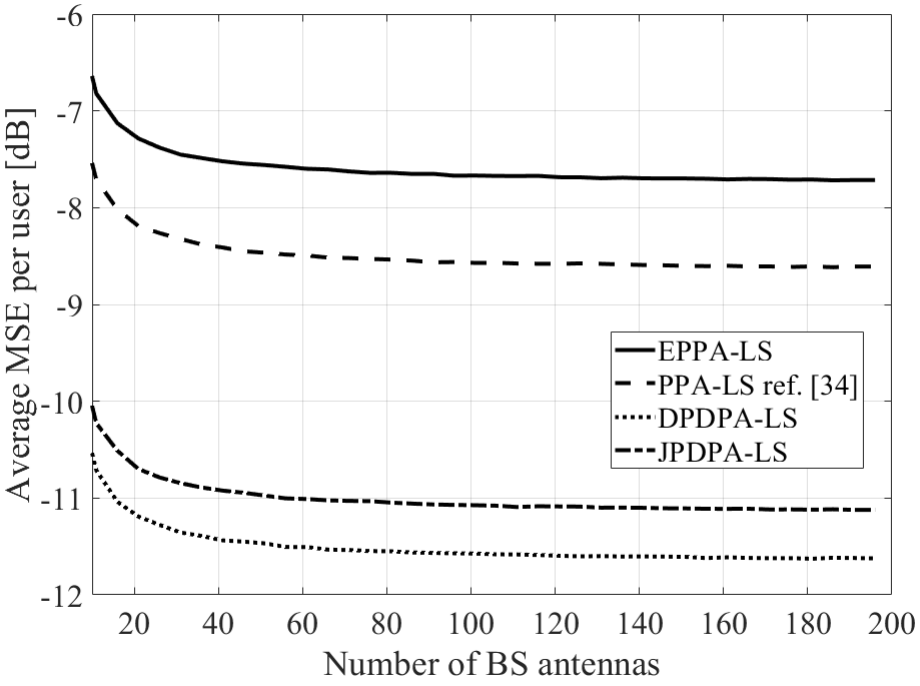

Figure 3.1: The average MSE per user versus the number of BS antennas M for LS channel estimator.

Fig. (3.1) shows the Monte-Carlo simulations of the average MSE channel estimation error for the LS channel estimation method. It can be seen clearly that the proposed approach DPDPA outperforms all three remaining approaches since

DPDPA can find the global minimization point for the sum of NMSE, while PPA in [34] only focuses on the sum MSE of one target cell and PPA is iteratively applied to other cells by using a cell grouping strategy. The gap between DPDPA and PPA is quite large with nearly 3 dB at $M = 200$. JPDPA is about 0.6 dB worse than our proposed method, since JPDPA uses the closed-from expression of the user SINR to find the optimized pilot power set instead of focusing directly on the NMSE closed form, which is the metric used to measure the channel estimation quality.

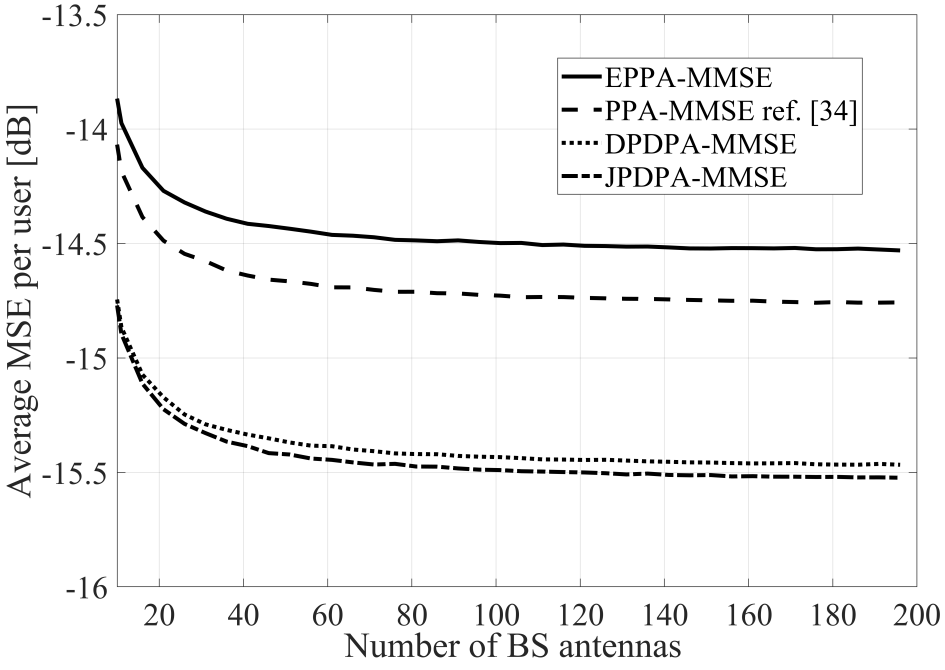

Figure 3.2: The average MSE per user versus the number of BS antennas M for MMSE channel estimator.

Similar to Fig. (3.1), Fig. (3.2) presents the simulation results for MMSE channel estimation. In this case, our proposed approach still performs much better than EPPA and PPA with the gap are nearly 1.5 dB and 1.2 dB at $M = 200$, respectively. How-

ever, the proposed DPDPA for MMSE is slightly worse than JPDPA since DPDPA only finds the local minimization point for the sum NMSE minimization problem. Furthermore, we do not simply stop at improving the channel estimation quality, but continue trying to directly improve the sum SE of the system; the simulation results for this will be presented in the following subsection.

3.4.2 Achievable rate evaluation

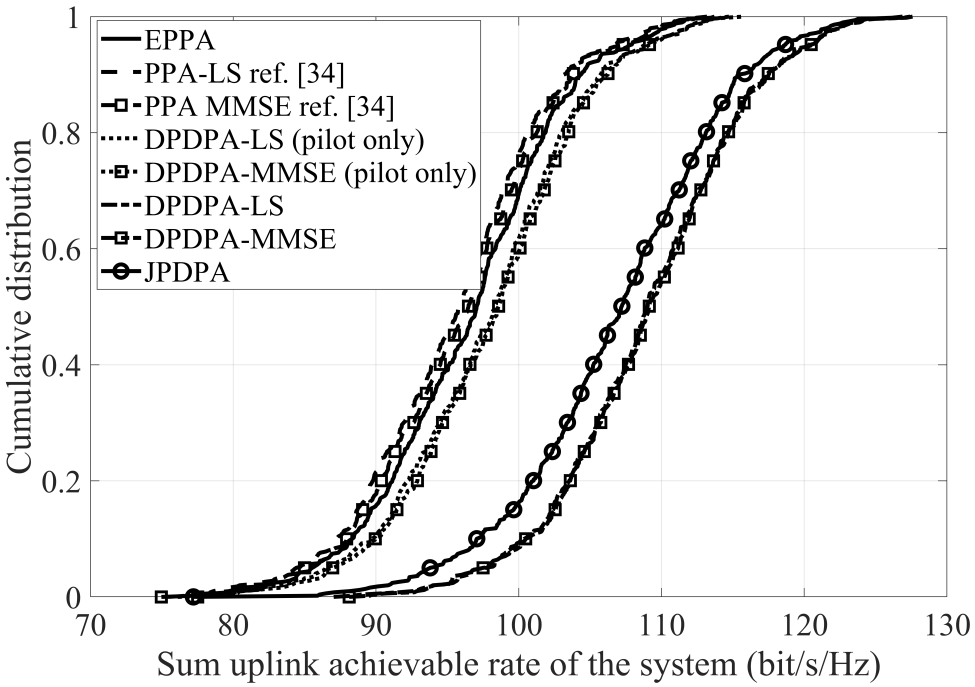

Figure 3.3: CDF of the sum uplink achievable rate of the system at $M = 200$.

In this subsection, we compare the uplink achievable rate of our proposed DPDPA with EPPA, PPA [34], JPDPA schemes and our DPDPA approach using only pilot power allocation (marked as "pilot only" in Figs. (3.3) and (3.4)) with the data power

of users assumed the same and are set to the max value $p_{kj}^{\max} = 300\text{mW}, \forall k, j$.

Fig. (3.3) gives the CDF of the sum uplink achievable rate of the system at $M = 200$ for the eight aforementioned approaches. First of all, the performance of MMSE is slightly better than LS for EPPA and DPDPA-pilot only, while the performances of LS and MMSE are nearly same for our proposed DPDPA approach. The reason is that EPPA and DPDPA-pilot only for MMSE has better channel estimation quality than for LS, and this results in a higher sum achievable rate for MMSE. However, the proposed DPDPA approach takes one more step to directly optimize the sum achievable rate and this step makes the gap between LS and MMSE methods almost negligible. It can be seen clearly that our DPDPA method outperforms the others with nearly 3 bit/s/Hz higher than JPDPA, 12 bit/s/Hz higher than DPDPA-pilot only and 15 bit/s/Hz higher than PPA and EPPA. DPDPA-pilot only still performs better than EPPA and PPA, which means that even without data power allocation, our proposed approach still performs better than the EPPA and PPA schemes. Futher, if we use DPDPA with disjoint pilot and data power allocation, the improvement is increased by 12 bit/s/Hz. Finally, the proposed DPDPA approach performs better than JPDPA because pilot and data power are optimized based on suitable objective functions, in contrast to JPDPA which uses one objective function for both the pilot and power allocation optimizations.

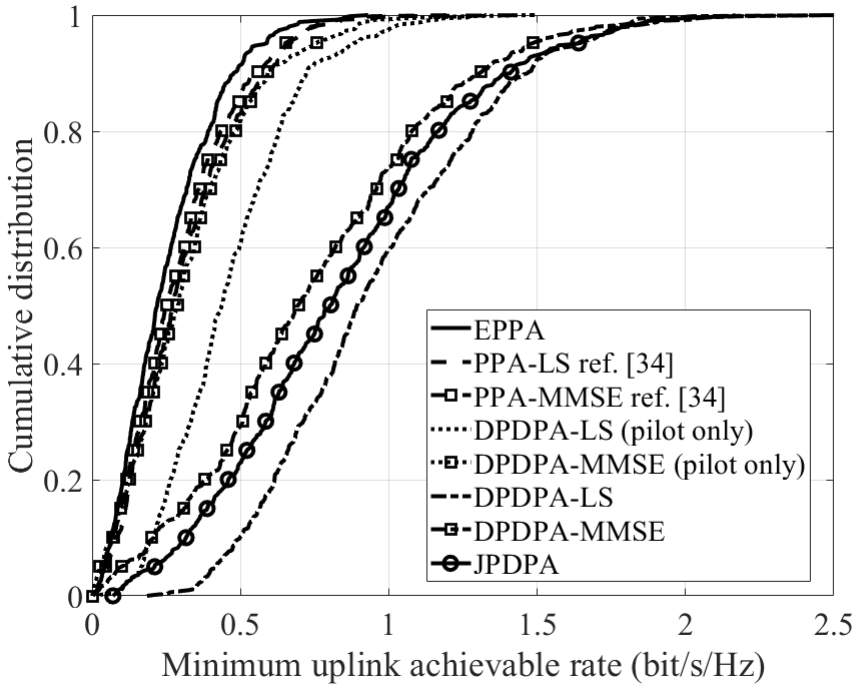

Figure 3.4: CDF of the minimum uplink achievable rate at $M = 200$.

Fig. (3.4) illustrates the CDF of the minimum uplink achievable rate of the system at $M = 200$ for the eight approaches. The minimum achievable rate is the highest for the proposed DPDPA-LS, where JPPDA is second and DPDPA-MMSE is third. DPDPA-pilot only for both LS and MMSE also improves the minimum achievable rate in comparison with PPA and EPPA. Moreover, the minimum achievable rate for LS is always better than for MMSE in PPA, DPDPA-pilot only and DPDPA approaches. This is because the LS method sees the co-channel interference (the interference from users in other cells which are assigned the same pilot) as noise while minimizing the sum NMSE of channel estimation errors will give more pilot power to the users who have bad channel estimation quality.

Chapter 4

Power allocation in multiple user-type system

4.1 Introduction and motivation

Most of power allocation schemes proposed in existing research works consider only one type of user so that they can only achieve one goal: providing uniform service for all users or maximizing the sum-rate of all users. The authors of [38] investigated the effectiveness of max-min fairness and maximized sum SE optimization problem in single-cell massive MIMO systems, and they derived a closed-form expressions for the user SE with pilot and data power as variables. The authors of [53] generalized the pilot design and uplink power allocation in one optimization problem and formulated a max-min fairness problem under a power budget constraint, with pilot signals and data power as variables. The authors of [54] considered the pilot and data power allocation to maximize the sum SE with two separate steps: the first step is to

indirectly improve sum SE by improving the channel estimation quality based on pilot power allocation, and the second step is to directly improve sum SE by optimizing the data power allocation. Power allocation schemes in [53] and [54] consider only one type of user so that they can only achieve one goal: providing uniform service for all users or maximizing the sum-rate of all users.

In this chapter, we propose a multiple user-type massive MIMO system and investigate the pilot and data power optimization in the proposed system model. The main contributions are summarized as follows.

- Unlike conventional massive MIMO systems in which all users belong to the same type, we propose a multiple user-type massive MIMO system that consists of two user types: QoS users who are guaranteed to have good and stable QoS, and non-QoS users who are similar to users in conventional systems with no guaranteed QoS.

- We formulate one power allocation optimization problem which guarantees QoS for QoS users and maximizes the sum-rate of non-QoS users simultaneously. Another power allocation optimization problem is proposed focusing on the same two targets as the previous one, but considering an additional aspect, which is energy efficiency (EE) of QoS users.

- Since both proposed optimization problems are non-convex and very hard to be solved directly, we propose two successive convex approximation algorithms to solve these two problems. We also prove that the proposed successive approximation algorithms converge at a local maximum Karush-Kuhn-Tucker (KKT) point.

4.2 Proposed multiple user-type system model

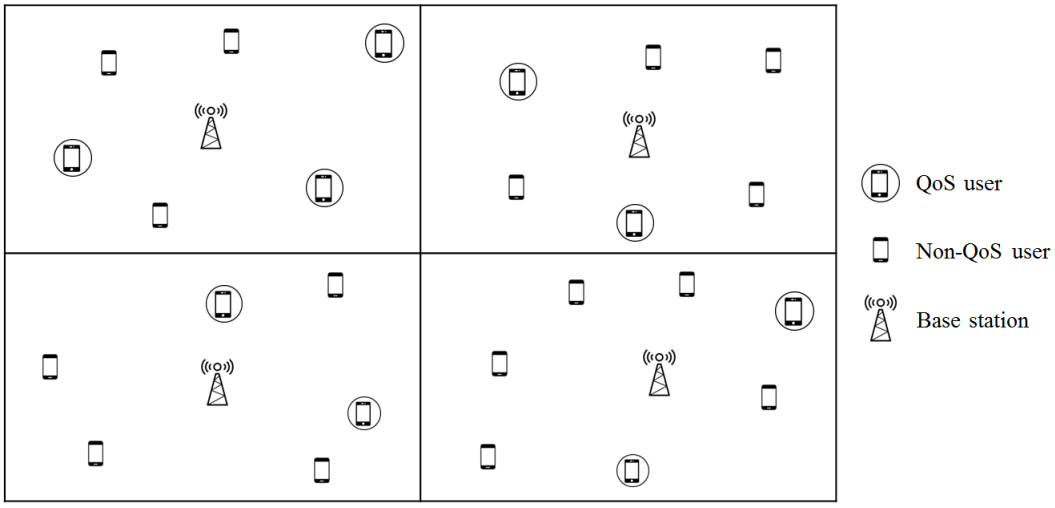

Figure 4.1: System model of the proposed multiple user-type massive MIMO systems.

Different from conventional massive MIMO systems [6] [10], in which all users are treated equally, in this chapter, we consider a massive MIMO system with two types of users, as shown in Fig.(4.1). The first type is non-QoS users who are similar to users in conventional massive MIMO systems; in other words, non-QoS users cannot be guaranteed to have QoS equal to or greater than a required value. The second type is QoS users, who are guaranteed the required QoS.

We consider a multi-cell multi-user multiple massive MIMO system with L cells. Each cell consists of a BS with M antennas and K ($M >> K$) users. In the proposed system, K users are composed of non-QoS users and QoS users. The system operates in TDD mode so that the channels in the uplink and downlink are reciprocal, which means we only need to estimate the uplink channels. The channel vector from user k

in cell j to the BS in cell l $\mathbf{h}_{kjl} \in C^{M\times 1}$ is:

$$\mathbf{h}_{kjl} = \mathbf{g}_{kjl}\sqrt{\beta_{kjl}}, \tag{4.1}$$

where $\mathbf{g}_{kjl} \sim CN(\mathbf{0}_{M\times 1}, \mathbf{I}_M)$ represents the small-scale fading and β_{kjl} is the large-scale fading coefficient. We assume block fading in which the large-scale fading changes slowly over many coherent time intervals, and thus can be easily tracked at the BS, while the small-scale fading does not change within one coherence interval [6].

More specifically, the channel considered in this chapter follows an uncorrelated Rayleigh fading model [52], where the channel matrices are simple diagonal matrix with the same value of all diagonal elements. Thanks to this channel matrix properties, our proposed method considers power allocation for the case of uncorrelated Rayleigh fading as number-based functions and optimizations. On the other hand, channel model in the case of spatially correlated Rayleigh fading [61] is more complicated and related to matrix-based calculus. Therefore, the proposed method in this case is not suitable.

4.2.1 Uplink training and MMSE channel estimation

BSs estimate user channels by using training signals (uplink pilot signals). We assume that τ_{c} is the length of one coherent interval, in which τ_{p} out of τ_{c} is used for the uplink pilot signals, and the remaining $\tau_{\mathrm{c}} - \tau_{\mathrm{p}}$ is for uplink data transmission. Due to the limited resources, a set of mutually orthogonal pilot sequences is reused in every cell so that there is no intra-cell pilot contamination. The set $\mathbf{\Psi}$ with the K

orthogonal pilots set is expressed as

$$\mathbf{\Psi} = [\psi_1, \psi_2, \ldots, \psi_K]^T \in C^{K \times \tau_{\mathrm{p}}}, \tag{4.2}$$

$$\psi_i^H \psi_i = \tau_{\mathrm{p}}, \psi_i^H \psi_j = 0, \forall i \neq j. \tag{4.3}$$

The BS in cell j receives the training pilot signal as

$$\mathbf{Y}_j = \sum_{i=1}^{L} \sum_{n=1}^{K} \sqrt{p_{ni}} \mathbf{h}_{nij} \psi_n^H + \mathbf{N}_j, \tag{4.4}$$

where $\mathbf{N}_j \in C^{M \times \tau_{\mathrm{p}}}$ denotes Gaussian noise at the BS in cell j with independent and identically distributed zero-mean and unit-variance elements, and p_{ni} is the pilot power of user n in cell i.

We calculate the estimated channel between the BS in cell j and user k in cell j. The received training signal in (4.4) is correlated with the k^{th} pilot as

$$\begin{aligned} \mathbf{y}_{kj} &= \mathbf{Y}_j \psi_k \\ &= \tau_{\mathrm{p}} \sqrt{p_{kj}} \mathbf{h}_{kjj} + \sum_{i \neq j}^{L} \tau_{\mathrm{p}} \sqrt{p_{ki}} \mathbf{h}_{kij} + \mathbf{n}_{kj}, \end{aligned} \tag{4.5}$$

where $\mathbf{n}_{kj} = \mathbf{N}_j \psi_k$ denotes the equivalent noise after being correlated with the pilot sequence, whose elements follow complex Gaussian distribution with zero-mean.

The MMSE estimated channel [41] between user k in cell j and the BS in cell j is calculated as

$$\hat{\mathbf{h}}_{kjj} = \frac{\sqrt{p_{kj}} \beta_{kjj}}{\sum_{i=1}^{L} \tau_{\mathrm{p}} p_{ki} \beta_{kij} + 1} \mathbf{y}_{kj}. \tag{4.6}$$

4.2.2 Uplink data and closed form SINR

After training phase, BSs use estimated channels to create a detector for detecting the uplink data signal. In this chapter, we use maximum ratio combining (MRC)

detector. The uplink data signal from user k in cell j detected at the BS in cell j is calculated as

$$\begin{aligned}\hat{d}_{kj} &= (\hat{\mathbf{h}}_{kjj})^H \Bigg(\sum_{l=1}^{L} \sum_{n=1}^{K} \sqrt{\rho_{nl}} \mathbf{h}_{nlj} d_{nl} + \mathbf{w}_j \Bigg) \\ &= \sqrt{\rho_{kj}} (\hat{\mathbf{h}}_{kjj})^H \mathbf{h}_{kjj} d_{kj} + \sum_{l=1}^{L} \sum_{n \neq k}^{K} \sqrt{\rho_{nl}} (\hat{\mathbf{h}}_{kjj})^H \mathbf{h}_{nlj} d_{nl} \\ &+ (\hat{\mathbf{h}}_{kjj})^H \mathbf{w}_j, \end{aligned} \tag{4.7}$$

where $d_{nl} \sim CN(0,1)$ is the uplink signal from user n in cell l, and ρ_{nl} is the average power of each symbol of data signal s_{nl}. $\mathbf{w}_j$ is Gaussian noise at the BS in cell j. Using the lower bounding technique on user SE as in [54, eq.(9)], the effective SINR for user k in cell j is given as

$$\text{SINR}_{kj} = \frac{A_{kj}}{B_{kj} - C_{kj} + D_{kj}}, \tag{4.8}$$

where

$$\begin{aligned} A_{kj} &= \rho_{kj} |\mathbf{E}\{(\hat{\mathbf{h}}_{kjj})^H \mathbf{h}_{kjj}\}|^2, \\ B_{kj} &= \sum_{l=1}^{L} \sum_{n}^{K} \rho_{nl} \mathbf{E}\{|(\hat{\mathbf{h}}_{kjj})^H \mathbf{h}_{nlj}|^2\}, \\ C_{kj} &= \rho_{kj} |\mathbf{E}\{(\hat{\mathbf{h}}_{kjj})^H \mathbf{h}_{kjj}\}|^2, \\ D_{kj} &= \mathbf{E}\{\|\hat{\mathbf{h}}_{kjj}\|^2\}. \end{aligned} \tag{4.9}$$

The closed form of SINR_{kj} is calculated as in [54, eq.(10)] and is given as

$$\text{SINR}_{kj} = \frac{X_{kj}}{Y_{kj} Z_{kj} + T_{kj}}, \tag{4.10}$$

where

$$\begin{aligned} X_{kj} &= Mp_{kj}\rho_{kj}\tau_{\mathrm{p}}(\beta_{kjj})^2, \\ Y_{kj} &= \sum_{l=1}^{L} p_{kl}\tau_p\beta_{klj} + 1, \\ Z_{kj} &= \sum_{l=1}^{L}\sum_{n=1}^{K} \rho_{nl}\beta_{nlj} + 1, \\ T_{kj} &= \sum_{l\neq j}^{L} Mp_{kl}\rho_{kl}\tau_{\mathrm{p}}(\beta_{klj})^2. \end{aligned} \tag{4.11}$$

4.3 Optimization problem formulation

In conventional massive MIMO systems, it is assumed that all users are treated equally and the network operator can provide the same QoS uniformly for all users [38], [53] or they can try to maximize the sum rate of all users in the systems [54]. In contrast, we consider a practical scenario when the network operators need to guarantee at least a required QoS for a portion of users. We call this type of user as QoS user. The remaining users are called non-QoS users and with this type of user, we do not need to guarantee any quality. Therefore, with non-QoS users, we seek to maximize their sum rate. In this section, we form the optimization problems to satisfy these two requirements at once.

4.3.1 Sum-rate maximization aspect

Let R_{kj} be the rate of user k in cell j, which is determined as

$$R_{kj} = \frac{\tau_c - \tau_p}{\tau_c}\log_2(1 + \mathrm{SINR}_{kj}). \tag{4.12}$$

Each QoS user is guaranteed a QoS ξ_{kj}, or in other words, $R_{kj} \geq \xi_{kj}, \forall k, j$, where

ξ_{kj} denotes the required quality that the system has to be able to provide user k in cell j. Besides guaranteeing QoS for QoS users, we also try to maximize the sum rate of non-QoS users. Motivated by that, the optimization problem for the multiple user-type massive MIMO systems is formulated as

$$\begin{aligned} \underset{\{\rho_{kj},p_{kj}\}}{\text{maximize}} \quad & \sum_{(k,j)\in\Gamma} R_{kj} \\ \text{subject to} \quad & R_{ml} \geq \xi_{ml}, \forall (m,l) \in \Omega, \\ & 0 \leq \rho_{kj} \leq \rho_{kj}^{\max}, \forall k, j, \\ & 0 \leq p_{kj} \leq p_{kj}^{\max}, \forall k, j, \end{aligned} \tag{4.13}$$

where $(k,j) \in \Gamma$ denotes that user k in cell j belongs to the set of non-QoS users Γ in the entire system, and $(m,l) \in \Omega$ denotes that the user m in cell l belongs to the set of QoS users Ω in the entire system.

4.3.2 Energy efficiency aspect

The solution of the previous optimization problem helps the network operator provide both a maximized sum-rate for non-QoS users and guaranteed QoS for QoS users. In this subsection, we consider an additional aspect, which is enhancing the energy efficiency (EE) in the proposed systems. From that, we formulate the second optimization problem considering three targets: guaranteeing QoS for QoS users, maximizing the sum-rate for non-QoS users and minimizing the power used by QoS

users. The second problem is given as

$$\begin{aligned} \underset{\{\rho_{kj},p_{kj}\}}{\text{maximize}} \quad & \sum_{(k,j)\in\Gamma} R_{kj} - \sum_{(m,l)\in\Omega} (p_{ml} + \rho_{ml}) \\ \text{subject to} \quad & R_{ml} \geq \xi_{ml}, \forall (m,l) \in \Omega, \\ & 0 \leq \rho_{kj} \leq \rho_{kj}^{\max}, \forall k, j, \\ & 0 \leq p_{kj} \leq p_{kj}^{\max}, \forall k, j, \end{aligned} \tag{4.14}$$

Specifically, maximizing the left part $\sum_{(k,j)\in\Gamma} R_{kj}$ is to maximize the sum-rate of all non-QoS users in the system. Simultaneously, maximizing the right part $-\sum_{(m,l)\in\Omega}(p_{ml} + \rho_{ml})$ is to minimize the total power used for pilot and data signals of QoS users.

4.4 Solution for problems

Since there are many variables $p_{kj}, \rho_{kj}, \forall k, j$ in both numerator and denominator of the SINR formulation, two proposed optimization problems in previous part are non-convex and difficult to directly solve. In this section, we propose solutions to approximately solve these two problems. In other word, the proposed solutions focus on finding local optimum points to these two proposed optimization problems.

4.4.1 First problem solution

We use the well-known lower bound on the natural logarithm function [63]:

$$a \ln(z) + b \leq \ln(1 + z). \tag{4.15}$$

This approximation is tight at a given $z = z_0$. The approximation constants are selected as

$$a = \frac{z_0}{1+z_0},\ b = \ln(1+z_0) - \frac{z_0}{1+z_0}\ln z_0. \tag{4.16}$$

We use this approximation in an iterative manner, which means at each iteration, we approximate rate R_{kj} by using the results from the previous iteration. Considering the approximation at the t^{th} iteration, each user rate R_{kj}^t is formulated as

$$\hat{R}_{kj}^t = \frac{\tau_\mathrm{c} - \tau_\mathrm{p}}{\tau_\mathrm{c}} \left(a_{kj}^t \ln \mathrm{SINR}_{kj} + b_{kj}^t \right) \log_2 e. \tag{4.17}$$

where a_{kj}^t, b_{kj}^t are the constant at the t^{th} iteration, calculated as in (4.16) by using the result from the previous $(t-1)^{th}$ iteration. The approximated optimization problem now becomes

$$\begin{aligned} \underset{\{\rho_{kj}, p_{kj}\}}{\text{maximize}} \quad & \frac{\tau_\mathrm{c} - \tau_\mathrm{p}}{\tau_\mathrm{c}} \left(\sum_{(k,j)\in\Gamma} \ln(\mathrm{SINR}_{kj})^{a_{kj}^t} \right) \log_2 e \\ \text{subject to} \quad & R_{ml} \geq \xi_{ml}, \forall (m,l) \in \Omega, \\ & 0 \leq \rho_{kj} \leq \rho_{kj}^{\max}, \forall k, j, \\ & 0 \leq p_{kj} \leq p_{kj}^{\max}, \forall k, j. \end{aligned} \tag{4.18}$$

We can remove the summation of all b_{kj}^t since they are constants, and we change constant a_{kj}^t to the exponent.

Since the natural logarithm is a non-decreasing function, the maximization of $\ln(f(x))$ is equivalent to the maximization of $f(x)$. Finally, we obtain the maximiza-

tion problem as

$$\begin{aligned} \underset{\{\rho_{kj},p_{kj}\}}{\text{maximize}} \quad & \prod_{(k,j)\in\Gamma} (\text{SINR}_{kj})^{a^t_{kj}} \\ \text{subject to} \quad & R_{ml} \geq \xi_{ml}, \forall (m,l) \in \Omega, \\ & 0 \leq \rho_{kj} \leq \rho^{\max}_{kj}, \forall k, j, \\ & 0 \leq p_{kj} \leq p^{\max}_{kj}, \forall k, j. \end{aligned} \tag{4.19}$$

The above maximization problem is not a formal convex form but it belongs to the geometric programming (GP) optimization problem class [43]. Since all variables p_{kj}, ρ_{kj} are non-negative, the numerator of the objective function is a monomial function, and the denominator is a posynomial function [43]. GP can be easily transformed into a convex problem by changing the variables to log domain, so that GP can be efficiently solved by many convex optimization solver computer programs such as SeduMi [44], MOSEK [46], or SDPT3 [45]. In the simulation of this chapter, we use the CVX high-level modeling frameworks [47] and MOSEK solvers in MATLAB.

To terminate the iterative algorithm, we use a termination condition value, which is calculated as the difference betweenthe values of the current and previous objective functions. When the termination condition value is smaller than or equal to a predefined threshold ϵ, we terminate the iteration process. In the simulation, we set $\epsilon = 0.01\%$.

The successive approximation to solve the proposed optimization problem is detailed in **Algorithm 1**.

Algorithm 3 Proposed Successive Approximation Algorithm for the First Problem

Initialize: $t = 0$, get $a_{kj}^t b_{kj}^t, \forall (k,j) \in \Gamma$ as in (4.16) with random $p_{kj}, \rho_{kj}, \forall k, j$.

Do

1: $t = t + 1$

2: Update $a_{kj}^t, b_{kj}^t \forall (k,j) \in \Gamma$ as in (4.16), using results at $(t-1)^{th}$ iteration.

3: Solve the approximated GP problem (4.19).

4: Check termination condition.

While (Not Converge)

Output: Optimal power set $p_{kj}, \rho_{kj}, \forall k, j$.

4.4.2 Second problem solution

In the second problem, if we only apply the approximation technique (4.15) as in the first problem, we get the problem below.

$$\begin{aligned} \underset{\{\rho_{kj}, p_{kj}\}}{\text{maximize}} \quad & \frac{\tau_{\mathrm{c}} - \tau_{\mathrm{p}}}{\tau_{\mathrm{c}}} \left(\sum_{(k,j)\in\Gamma} \ln(\mathrm{SINR}_{kj})^{a_{kj}^t} \right) \log_2 e \\ & - \sum_{(m,l)\in\Omega} (p_{ml} + \rho_{ml}) \\ \text{subject to} \quad & R_{ml} \geq \xi_{ml}, \forall (m,l) \in \Omega, \\ & 0 \leq \rho_{kj} \leq \rho_{kj}^{\max}, \forall k, j, \\ & 0 \leq p_{kj} \leq p_{kj}^{\max}, \forall k, j, \end{aligned} \tag{4.20}$$

This optimization problem cannot be transformed into GP since it is in a subtractive form. We take a further step by changing the domain of all variables to an exponential domain. Let $p_{kj} = e^{\tilde{p}_{kj}}, \rho_{kj} = e^{\tilde{\rho}_{kj}}, \forall k, j$. Replace the new variables $\tilde{p}_{kj}, \tilde{\rho}_{kj}$ into (4.20), the final approximated problem is given as

$$\begin{aligned}
\underset{\{\rho_{kj},p_{kj}\}}{\text{maximize}} \quad & \frac{\tau_{\mathrm{c}}-\tau_{\mathrm{p}}}{\tau_{\mathrm{c}}} \sum_{(k,j)\in\Gamma} \Bigg(\ln\left(M\tau_{\mathrm{p}}(\beta_{kjj})^2\right)(\tilde{p}_{kj}+\tilde{\rho}_{kj}) - \\
& \ln\Bigg(\Bigg(\sum_{l=1}^{L} e^{\tilde{p}_{kl}}\tau_{\mathrm{p}}\beta_{klj}+1\Bigg)\Bigg(\sum_{l=1}^{L}\sum_{n=1}^{K} e^{\tilde{\rho}_{nl}}\beta_{nlj}+1\Bigg) \\
& + \sum_{l\neq j}^{L} M e^{\tilde{p}_{kl}} e^{\tilde{\rho}_{kl}} \tau_{\mathrm{p}}(\beta_{klj})^2\Bigg)\Bigg)\log_2 e - \sum_{(m,l)\in\Omega}(e^{\tilde{p}_{ml}}+e^{\tilde{\rho}_{ml}}) \\
\text{subject to} \quad & R_{ml} \geq \xi_{ml}, \forall (m,l)\in\Omega, \\
& 0 \leq \rho_{kj} \leq \rho_{kj}^{\max}, \forall k,j, \\
& 0 \leq p_{kj} \leq p_{kj}^{\max}, \forall k,j,
\end{aligned}$$

Since exp and the second ln function (ln −sum−exp) are convex, the maximization problem (4.21) is convex. Once again, we can use any convex solver computer program to solve this optimization problem. The details of **Algorithm 2** for solving the second optimization problem are presented below.

Algorithm 4 Proposed Successive Approximation Algorithm for the Second Problem

Initialize: $t=0$, get $a_{kj}^t b_{kj}^t, \forall (k,j)\in\Gamma$ as in (4.16) with random $p_{kj}, \rho_{kj}, \forall k,j$.

Do

1: $t=t+1$

2: Update $a_{kj}^t, b_{kj}^t \forall (k,j)\in\Gamma$ as in (4.16), using result from $(t-1)^{th}$ iteration.

3: Change the variables to log domain as $p_{kj}=e^{\tilde{p}_{kj}}, \rho_{kj}=e^{\tilde{\rho}_{kj}}, \forall k,j$.

4: Solve the convex problem (4.21) with new variables.

5: Map back to original variables.

6: Check termination condition.

While (Not Converge)

Output: Optimal power set $p_{kj}, \rho_{kj}, \forall k,j$.

4.4.3 Discussion on convergence and complexity

Convergency property

Using the general approximation framework [48] as in [53] [54], we propose the following lemma:

Lemma 1: *The two proposed successive approximation algorithms adapt the general inner approximation algorithm for the non-convex optimization problem [48], and satisfy three conditions:*

- $f(\mathbf{x}) \leq \tilde{f}(\mathbf{x})$ *for all feasible* $\mathbf{x}$*,*
- $f(\mathbf{x}_0) = \tilde{f}(\mathbf{x}_0)$*,* $\mathbf{x}_0$ *is the optimal point of the approximated problem from the previous iteration,*
- $\nabla f(\mathbf{x}_0) = \nabla \tilde{f}(\mathbf{x}_0)$*,*

where $f(\mathbf{x})$ *is the original non-convex function and* $\tilde{f}(\mathbf{x})$ *is the approximated convex one. Three conditions guarantee that the two algorithms are going to converge to a local maximum Karush-Kuhn-Tucker (KKT) point.*

Proof: This proof derives from the general approximation framework in [48]. We denote the feasible set of the optimization problem (4.13) as

$$F = \{\rho_{kj}, p_{kj} | \forall k, j : \rho_{kj}, p_{kj} \in \mathbb{R}_+, \rho_{kj} \leq \rho_{kj}^{\max}, p_{kj} \leq p_{kj}^{\max}\}. \tag{4.21}$$

At the t^{th} iteration, the optimal solution to the approximated optimization problem (4.18) is denoted as

$$P^t = \{\rho_{kj}^{t,opt}, p_{kj}^{t,opt} | \forall k, j\}. \tag{4.22}$$

Let denote $R_{kj}(f)$ is the rate computed for any feasible point $f \in F$, and $\hat{R}^t_{kj}(P^t)$ is approximated rate at t^{th} iteration computed from (4.18) using the solution P^t obtained at the t^{th} iteration. By using the lower bound on natural logarithm function [63] as in (4.15), the family of all rate functions R_{kj} satisfies the properties belows:

$$\begin{aligned} &\hat{R}^t_{kj}(f) \leq R_{kj}(f), \forall f \in F, \\ &R_{kj}(P^t) = \hat{R}^{t+1}_{kj}(P^t), \\ &\frac{\partial R_{kj}(P^t)}{\partial \rho_{kj}} = \frac{\hat{R}^{t+1}_{kj}(P^t)}{\partial \rho_{kj}}, \\ &\frac{\partial R_{kj}(P^t)}{\partial p_{kj}} = \frac{\hat{R}^{t+1}_{kj}(P^t)}{\partial p_{kj}}. \end{aligned} \tag{4.23}$$

The first property in (4.23) ensures that the optimal objective value to the approximated problem (4.18) is also feasible for the original problem (4.13). From that, we construct the chain of inequalities as follows.

$$\cdots = \hat{R}^t_{kj}(P^{t-1}) \leq \hat{R}^t_{kj}(P^t) \leq R_{kj}(P^t) = \hat{R}^{t+1}_{kj}(P^t) \leq \ldots, \tag{4.24}$$

where the first inequality is obtained by solving the approximated problem (4.18). The second inequality follows the first property in (4.23) and the third equality follows the second property in (4.23).

From this chain, we observe that the objective function is non-decreasing with the iteration index t while the family of rate functions R_{kj}, for all k, j, is continuous function since pilot power ρ_{kj} and data power p_{kj} belong to continuous ranges of positive real values.

From the above observation, the proposed approximation method to solve (4.13) by the approximated problem (4.18) ensures the convergence. If the convergence occurs at the t^{th} iteration, then the optimal set P^t should also be a solution in the

$(t+1)^{th}$ iteration or the objective value at t^{th} iteration is equal to the one at $(t+1)^{th}$ iteration. Otherwise, the objective value should increase after each iteration. Moreover, the constraints in (4.13) and (4.18) satisfy Slater's condition [64] and guarantee that KKT conditions are hold if we use the last two properties in (4.23) to do a matching procedure as proved in [48]. In conclusion, the convergence point obtained by iteratively solving problem (4.18) is a KKT local point to problem (4.13).

Computational complexity

Since the most complex parts in the two proposed algorithms lie in GP or the convex problem at each iteration, we analyze the computational complexity of the two problems as follow.

Both problems have $2KL$ variables and $2KL+|\Omega|$ constraints, where $|\Omega|$ is the total number of QoS users in the system. Thus, as in [64], the computational complexity in one iteration is given as

$$\max\{(2KL)^3, (2KL)^2(2KL+|\Omega|), F_{\text{joint}}\}, \tag{4.25}$$

where F_{joint} is the cost of evaluating the first and second derivatives of the objective and constraints functions.

We can also see that **Algorithm 2** has more computational complexity than **Algorithm 1** since we need more steps to change the domain of the variable and the objective function in **Algorithm 2** is more complex than in **Algorithm 1**.

4.4.4 Applicability to ZF detector

In this subsection, we show that the proposed method can be applied to the case when ZF detector is used for uplink data detection instead of MRC. ZF is also a simple linear detector which can be used in massive MIMO systems. When the number of BS antennas is not so large (a few hundreds), ZF shows better performance as compared to MRC. However, the complexity of MRC is reduced by around 10% as compared to ZF since MRC requires no matrix inversions. More details about complexity and performance comparison between ZF and MRC have been provided in [52, subsection 4.1.4].

Lemma 2. *[58, Corollary 1] The closed-form SINR of user k in cell j is given as (4.26) at the top of next page. The parameter G and z_{kij} depend on the chosen detector, MRC or ZF. Then $G = M, z_{kij} = \beta_{kij}$ for MRC, and $G = M - K, z_{kij} = \beta_{kij}(1 - \frac{\rho_{ki}\tau_p\beta_{kij}}{\sum_{i=1}^{L}\rho_{ki}\tau_p\beta_{kij}+1})$ for ZF.*

With MRC, replacing $G = M, z_{kij} = \beta_{kij}$ into (4.26), we achieve exactly the same closed-form SINR as equation (4.10) as

$$\mathrm{SINR}_{kj} = \frac{Gp_{kj}\beta_{kjj}\frac{\rho_{kj}\tau_p\beta_{kjl}}{\sum_{i=1}^{L}\rho_{ki}\tau_p\beta_{kij}+1}}{G\sum_{i\neq j}^{L}p_{ki}\beta_{kij}\frac{\rho_{ki}\tau_p\beta_{kij}}{\sum_{n=1}^{L}\rho_{kn}\tau_p\beta_{knj}+1} + \sum_{i=1}^{L}\sum_{k=1}^{K}p_{ki}z_{kij} + 1} \tag{4.26}$$

Similarly, the closed-form SINR for ZF is given as

$$\mathrm{SINR}_{kj}^{ZF} = \frac{A_{kj}}{B_{kj} + C_{kj} + D_{kj}}, \tag{4.27}$$

where

$$\begin{aligned} A_{kj} &= (M-K)p_{kj}\rho_{kj}\tau_{\mathrm{p}}\beta_{kjj}^2, \\ B_{kj} &= (M-K)\sum_{i\neq j}^{L}\rho_{ki}p_{ki}\tau_p\beta_{kij}^2, \\ C_{kj} &= \sum_{i=1}^{L}\sum_{k=1}^{K}p_{ki}\beta_{kij}(\sum_{m\neq i}^{L}\rho_{km}\tau_p\beta_{kmi}+1), \\ D_{kj} &= \sum_{i=1}^{L}\rho_{ki}\tau_p\beta_{kij}+1. \end{aligned} \tag{4.28}$$

SINR_{kj}^{ZF} has the same structure as the case of MRC where the numerator is monomial function and the denominator is posynomial function. Consequently, when applying the proposed method to the case of ZF, the maximization problem (4.19) also belongs to the geometric programming (GP), as same as in the case of MRC. As a result, the proposed power allocation methods are able to be applied in the case of ZF detector.

4.5 Numerical results

We consider a multiple user-type massive MIMO system with $L = 4$ square cells covering a 500 m^2 area. Each cell has a BS at the center serving $K = 6$ users, simultaneously. Users are located randomly and uniformly in the cell, with the distance is not less than 35m from the BS. A wrap-around topology [38] [53] is used to simulate that all BSs have roughly equal interference from all directions. In each cell, half of the total users are QoS users and the remaining are non-QoS users. We consider this balance between QoS and non-QoS users to see clearly the performance of the proposed algorithms. In an extreme case when all K users are non-QoS users, the proposed problem becomes a sum-rate maximization problem as in [54]. In another

extreme case when all of K users are QoS users, the proposed problem becomes a max-min problem as in [38] [53].

The coherence interval is 200 symbols and the system bandwidth is 20 MHz. The noise variance is -94 dBm. The large-scale fading coefficient is calculated following the 3GPP LTE model [8] as

$$\beta_{ki}^{j} = -35.3 - \gamma \log_{10}(d_{ki}^{j}) + z_{ki}^{j}, \tag{4.29}$$

where -35.3 is the average channel gain in dB at a reference distance of 1 m, and $\gamma = 3.76$ represents the path-loss exponent. d_{ki}^{j} is the distance between user k in cell i and the BS cell j in meters. z_{ki}^{j} denotes the shadow fading following a log-normal distribution with a standard deviation of 5 dB. The maximum pilot and data powers for every user are $p_{kj}^{\max} = \rho_{kj}^{\max} = 300$ mW, $\forall k, j$.

Figure (4.2) illustrates the cumulative distribution function (CDF) of the uplink sum-rate of non-QoS users in the systems with different numbers of BS antennas $M = 100$, 200, & 300 and the required QoS for every QoS user is $\xi_{ml} = 2$ bit/s/Hz, $\forall (m, l) \in \Omega$. We denote the conventional equal power scheme as "EPS [53] [54]", and the first proposed algorithm as "Pro. no EE". $p_{kj}^{\max} = \rho_{kj}^{\max} = 300$mW, $\forall k, j$.

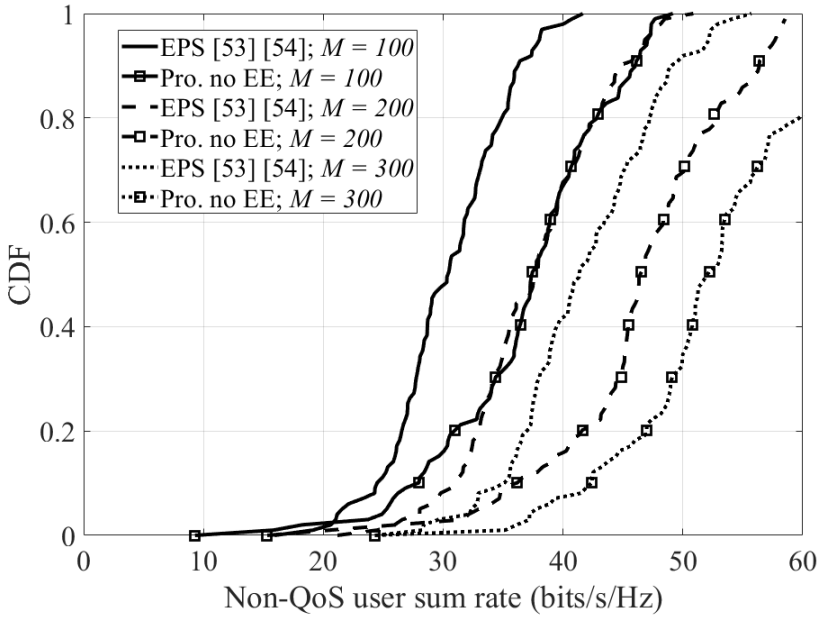

Figure 4.2: CDF of the sum-rate of non-QoS users with $\xi_{ml} = 2$ bit/s/Hz, $\forall (m, l) \in \Omega$.

It can be seen that the first proposed algorithm significantly improves the sum-rate of non-QoS users with more than 10 bit/s/Hz. Interestingly, when M increases, both EPS and the proposed scheme's performance also increase. This is because M increases means the degrees-of-freedom of channel vectors also increases. This makes the channel estimation quality better and leads to an enhanced rate.

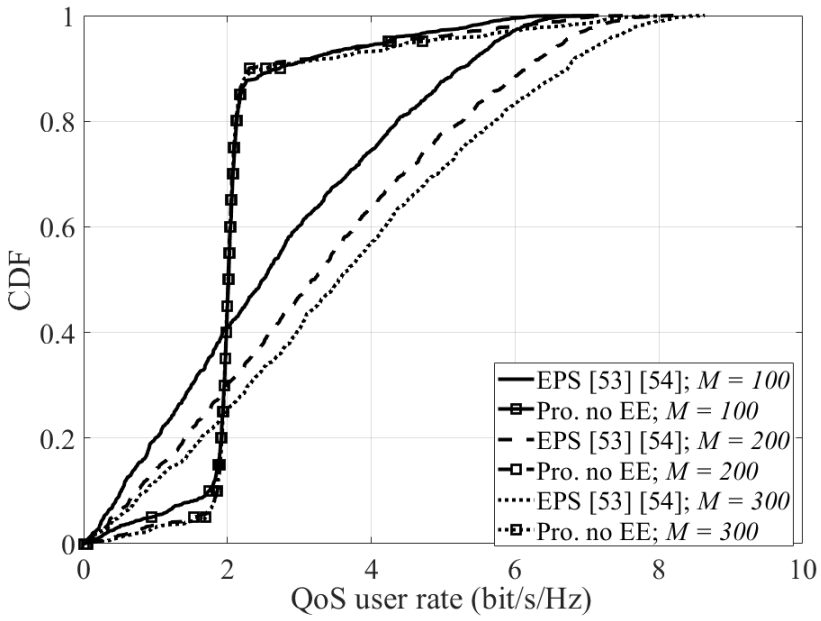

Figure 4.3: CDF of QoS users rate with $\xi_{ml} = 2$ bit/s/Hz, $\forall(m,l) \in \Omega$.

Figure (4.3) shows the CDF of the QoS user rate in the system with a different value of M and $\xi_{ml} = 2$ bit/s/Hz, $\forall(m,l) \in \Omega$. The QoS user rate in EPS covers a wide range from 0 to 8 bit/s/Hz. This phenomenon is actually bad since some QoS users have an unnecessarily too high rate while others have too low rate. In contrast, the first proposed algorithm helps to maintain the stable and good QoS among QoS users, and the simulation result in fig. 3 shows that almost all QoS users have a similar rate of about 2 bit/s/Hz. This is a uniformly good service for all QoS users, who in practical scenario, should pay more money than other users to have good and stable service.

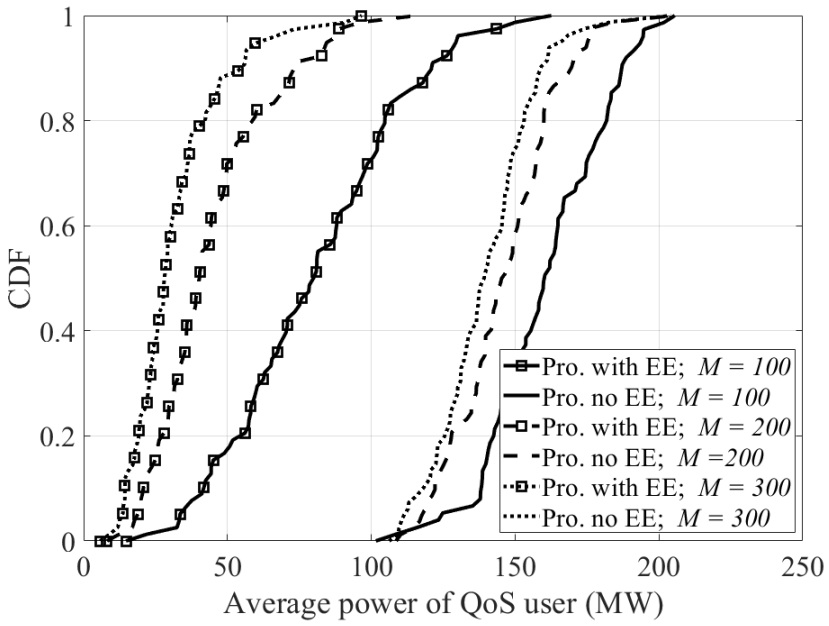

Figure 4.4: CDF of average power of QoS users.

Figure (4.4) shows the simulation results of the first and second proposed algorithms, marked as "Pro. no EE" and "Pro. with EE" respectively, in terms of the CDF of the average QoS user power. The average power used in the second algorithm is reduced much more than in the first one, with more than 75 mW at $M = 100$ and 100 mW at $M = 200$ and 300. This reduction happens since EE is not considered in the first algorithm. The first proposed algorithm only tries to maximize the sum-rate of non-QoS users and guarantees that the QoS users rate is at least $\xi_{ml} = 2$ bit/s/Hz. However, some QoS users have very good channel conditions and apparently they will have unnecessarily too high rate. The second algorithm tries to reduce the power of these aforementioned QoS users to improve EE. Better EE comes with the trade-off that the computational complexity of the second proposed algorithm is higher.

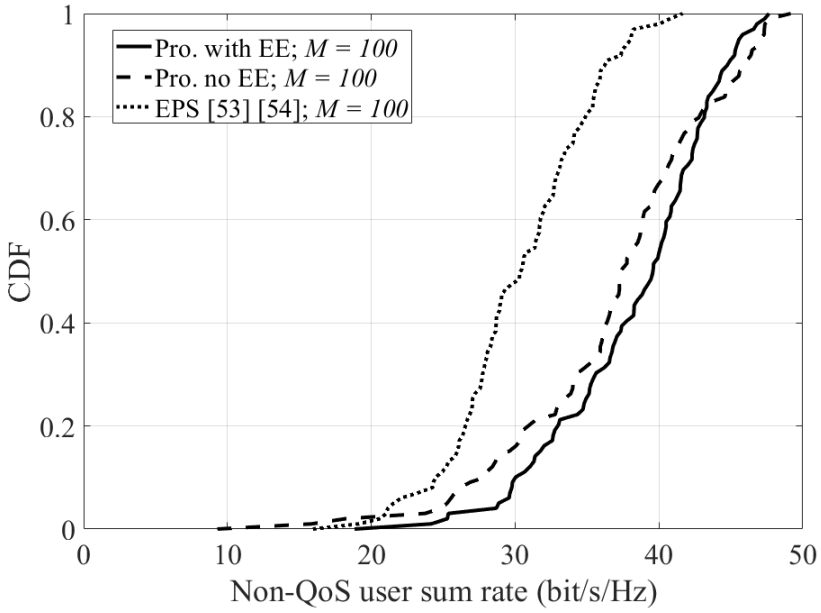

Figure 4.5: CDF of the sum-rate of non-QoS users with $M = 100$, $\xi_{ml} = 2$ bit/s/Hz, $\forall(m,l) \in \Omega$.

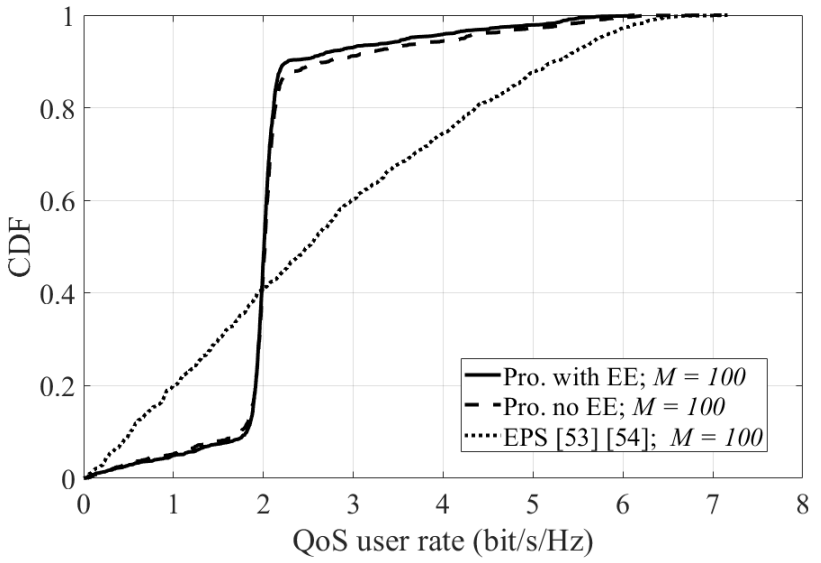

Figure 4.6: CDF of QoS users rate with $M = 100$, $\xi_{ml} = 2$ bit/s/Hz, $\forall(m,l) \in \Omega$.

Figures (4.5) and (4.6) show the CDF comparison between the first and second proposed algorithm in terms of non-QoS user's sum-rate and QoS user rate, respectively. With two proposed algorithms, around 90% of QoS user rates are 2 bit/s/Hz. In other words, two proposed algorithms provide very stable service for QoS users. In contrast, with EPS scheme, QoS user rates lie in a wide range, from 0 to 6 bit/s/Hz. This means the service provides to QoS users is unstable and varies too much. Moreover, it can be seen clearly that although the second proposed algorithm has to take into account EE, its effectiveness on non-QoS user sum-rate and QoS users rate is nearly the same as the first proposed algorithm.

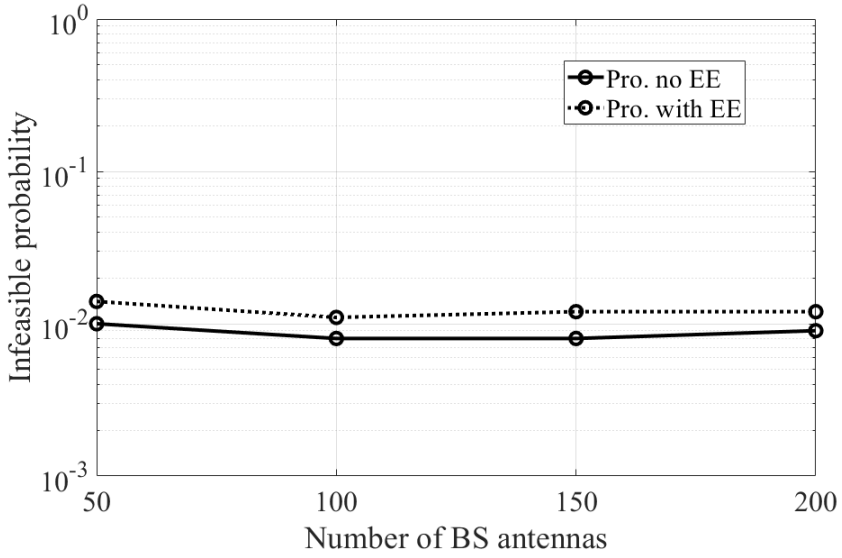

Figure 4.7: Infeasible probability versus different number of BS antennas with QoS = 2 (bit/s/Hz).

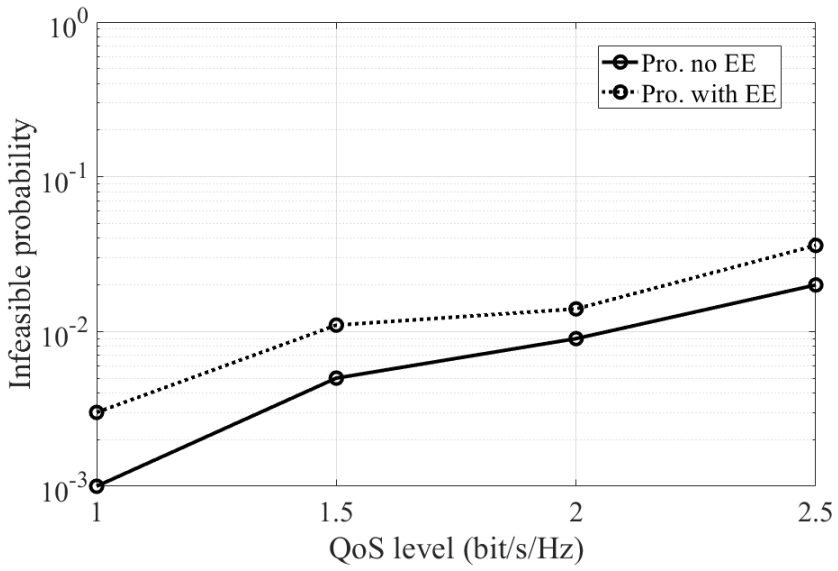

Figure 4.8: Infeasible probability versus different QoS level with number of BS antennas $M = 100$.

Figures (4.7) and (4.8) demonstrate the infeasible probability, which is calculated as the ratio between number of user location realization and number of times when the optimization problems are infeasible. From figure 7, we can see that the probability when infeasible issue happens does not affect when number of BS antennas M varies. This is obvious since M only plays as a constant in two proposed problems. In addition, the infeasible probability for the proposed algorithm without EE is better than the case with EE since we have to care more about energy efficiency in the latter case. Moreover, when the QoS level increases, the infeasible probabilities for both algorithms also increase as figure 8 shows. It is because when QoS level increases, there are more users with bad channel can not satisfy this QoS constraint and this makes problems infeasible. As addressed before, we would like to deeply investigate on feasibility issue in future works.

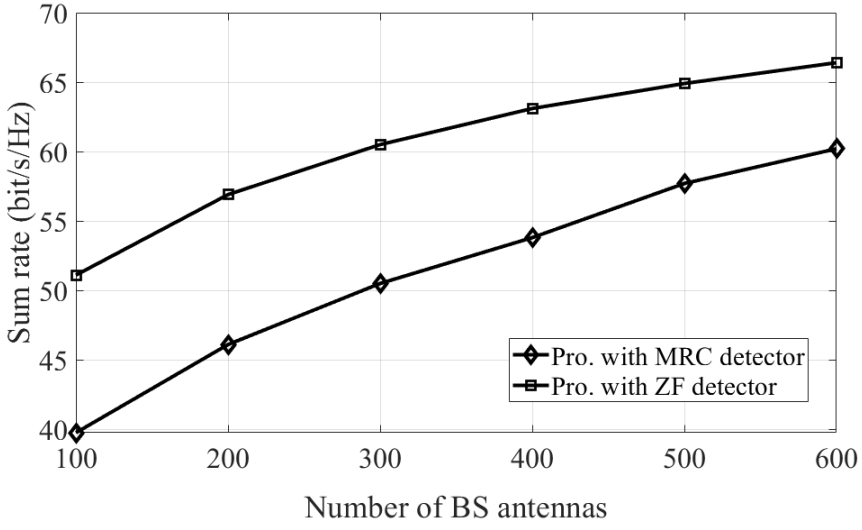

Figure 4.9: Sum rate of non-QoS users with various number of BS antennas.

Fig. (4.9) shows the achievable sum rate of non-QoS users with increasing number of BS antennas in two cases: MRC detector and ZF detector. Obviously, ZF provides better performance as compared to MRC, and this gap is around 10 bit/s/Hz when the number of BS antennas M is from 100 to 300. However, this advantage comes with a drawback that the complexity of ZF is 10% higher than MRC [12] since ZF has to calculate matrix inversion. Interestingly, when the number of BS antennas increases to from 400 to 600, the gap between MRC and ZF is getting narrower, thanks to the effect of channel hardening and favorable propagation, while the complexity of ZF keeps increasing much higher than MRC due to the increase of channel matrix size. Since we only focus on power allocation method, not on comparing between different detectors, interesting readers can find more details about this comparison on [52, subsection 4.1.4].

Chapter 5

Summary of contributions and future works

5.1 Thesis conclusion

A huge demand for data throughput is required in future cellular networks, because of the significant growing in number of wireless devices such as smart phone, tablet, internet of thing (IoT) devices and so on. Motivated by that, massive MIMO technology has been introduced and investigate by many reasearchers over the last few years. Massive MIMO is refered as it can bring a significant improvement in data throughput by increasing the system spectral efficiency (bit/s/Hz), while remaining the same density of base station per area unit and the same bandweidth. The extraordinary advantages can be obtained by increasing the number of bases station antennas to hundreds or more, to enable spatial multiplexing and array gain from user terminals.

Besides the undeniable advantages, massive MIMO technology also has some limiting issues that should be deeply investaged to mitigate. Pilot contamination is one of the important issue due to the lack of resource for channel estimation at base station. Moreover, the huge number of base station antennas and user equipments also raise an issue of allocating power efficiently. In this thesis, we investgate mainly on pilot contamination and power allocation problems. The main contributions of the dissertation is listed up as follows.

- First, we investigate the pilot contamination problem in massive MIMO systems with multi-path channel model. We point out that the interference between users with the same pilot sequence can be considered as a vertex graph. Therefore, we propose a metric which can roughly measure the interference and from that we can create an interference graph between any two users in the system. Consequently, pilot contamination can be mitigated by smartly assign pilot to each users by applying a classsic vertex graph coloring algorithm, in stead of randomly assigning pilot to user.

- Next, we study pilot power allocation problem to reduce the pilot contamination problem and to increase the sum achievable rate of the massive MIMO systems. Conventionally, pilot power is the same for all users, and we realize that this approach is not efficient since the channel quality of each user is different. Therefore, different and suitable power should be assigned to each user. Our scheme is divided into two separate parts: first part is pilot power allocation to improve the channel estimation quality and second part is data power allocation to increase the sum spectral efficiency. Each part has a correspond-

ing optimization problems to solve. One of problem is based on a exact form of channel estimation error, and the other one is based on sum spectral efficiency of all users in ther system.

- Finally, we observe that most of power allocation algorithm existing only focus on one user-type. In other words, all users in the system have the same roles. Therefore, only one target can be achieved for all users: faireness between all user or maximizing sum rate of all users. Inspired by that, we investigate pilot and power allocation optimization in a multiple user-type massive MIMO system. This proposed system have two types of users: non-QoS users who are the same with users in conventional massive MIMO system with no guaranty of QoS, and QoS users who are guaranteed to achieve a good and stable predefined QoS level. Eventually, two different optimizations problems and two according solving algorithms for each type of users are proposed.

5.2 Future research directions

Desipte the fact that massive MIMO has gain a lot of attention by researchers in the last few years, many interesting aspects of massive MIMO still remain to be investigated. There is still a lot of room to deeply dig in the problem pilot design instead of conventional orthogonal pilot, or new channel estimation technique which is suitable for the large-scale channel matrices and vectors in massive MIMO systems.

One of the interesting massive MIMO related topic is cell-free massive MIMO, which actually is a variant of conventional massive MIMO systems. In cell-free mas-

sive MIMO, there is no cell boundary between base stations. Consequently, one base station can support all users in the networks.

Another emerging topic is adapting machine learning and deep learning into massive MIMO system to enhance the channel estimation quality and to allocate power in more efficient and smart way.

Currently, we keep investigating to find better solutions for some proposed power allocation algorithms. Our target is to find new solution which is more accurate, less complex so that it can run faster to adapt better to the mobility property of cellular networks. Moreover, we are studing the problem of assigning connections and power between users and base station, which is very important in cell-free massive MIMO system due to the property of no cell bounder. Finally, deep learning based massive MIMO system is our ongoing topic in near future.

Publications

SCI(E) Journals

[1] **H. T. Dao** and S. Kim, "Vertex graph-coloring-based pilot assignment with location-based channel estimation for massive MIMO systems," *IEEE Access*, vol. 6, pp. 4599–4607, Jan. 2018.

[2] **H. T. Dao** and S. Kim, "Pilot power allocation for maximising the sum rate in massive MIMO systems," *IET Commun.*, vol. 12, no. 11 pp. 1367–1372, Jun. 2018.

[3] **H. T. Dao** and S. Kim, 'Worst cell based pilot allocation in massive MIMO systems," *MDPI Electronics*, vol. 7, no. 197 pp. 1–11, Sept. 2018.

[4] **H. T. Dao** and S. Kim, "Disjoint pilot power and data power allocation in multi-cell multi-user massive MIMO systems," *IEEE Access*, vol. 6, pp. 66513–66521, Oct. 2018.

[5] **H. T. Dao** and S. Kim, "Multiple-symbol non-coherent detection for differential QAM modulation in uplink massive MIMO systems," *MDPI Electronics*, vol. 8, no. 693 pp. 1–9, Jun. 2019.

[6] **H. T. Dao** and S. Kim, "Effective channel gain-based access point selection in

cell-free massive MIMO systems," *IEEE Access*, vol. 8, pp. 108127–108132, Jun. 2020.

[7] **H. T. Dao** and S. Kim, "Power allocation for multiple user-type massive MIMO systems," *IEEE Trans. Vehi. Tech.*, vol. 69, no. 10, pp. 10965–10974, Oct. 2020.

[8] **H. T. Dao** and S. Kim, 'Power allocation and user-AP connection in distributed massive MIMO systems," *IEEE Commun. Lett.*, vol. 25, no. 2, pp. 565–569, Feb. 2021.

International Conferences

[9] **H. T. Dao** and S. Kim, "Pilot power allocation for enhancing channel estimation quality in multi-cell multi-user massive MIMO systems," in Proc. Asia-Pacific Conf. on Commun. (APCC), Ho Chi Minh, Vietnam, 2019, pp. 207–210.

References

[1] Ring, D. H., *Mobile Telephony - Wide Area Coverage*, Bell Laboratories Technical Memorandum, 1947.

[2] Frefkiel, R. H., "A high-capacity mobile radiotelephone system modelusing a coordinated small-zone approach," *IEEE Trans. Veh. Technol*, 19(2): 173177, 1970.

[3] Young, W. R., "Advanced mobile phone service: Introduction, background, and objectives," *Bell System Technical Journal,* 58(1): 114, 1979.

[4] Shannon, C. E., "Communication in the presence of noise," *Proc. IRE*, 37(1): 1021, 1949.

[5] Tse, D. and P. Viswanath., *Fundamentals of wireless communications*, Cambridge University Press.,2005

[6] T. L. Maezetta, "Noncooperative cellular wireless with unlimited numbers of base station antennas," *IEEE Trans. Wireless Commun.*, vol. 9, no. 11, pp. 3590–3600, Nov. 2010.

[7] T. L. Maezetta and A. Ashikhmin, "MIMO system having a plurality of service

antennas for data transmission and reception and method thereof," *US Patent. 8594215*, 2011.

[8] *Further advancements for E-UTRA physical layer aspects (Release 9),* 3GPP TS 36.814, 2010.

[9] E. Bjrnson, E. G. Larsson, and M. Debbah, "Massive MIMO for maximal spectral efficiency: How many users and pilots should be allocated?," *Trans. Wireless Commun.*, vol. 15, no. 2, pp. 1293–1308, Feb 2016.

[10] F. Rusek, D. Persson, and B. Lau, "Scaling up MIMO: opportunities and challenges with very large arrays," *IEEE Signal Process. Mag.*, vol. 30, no. 1, pp. 40–60, Dec. 2012

[11] H. Ngo, E. Larsson, and T. Marzetta, "Energy and spectral efficiency of very large multiuser MIMO systems," *IEEE Trans. Commun.*, vol. 61, no. 4, pp. 1436–1449, Feb. 2013

[12] D. Arujo, T. Masksymyuk, and A. Almeida, "Massive MIMO: survey and future research topics," *IET Commun.*, vol. 10, no. 15, pp. 1938–1946, Oct. 2016

[13] J. Jose, A. Ashikhmin, and T. Marzetta, "Pilot contamination and precoding in multi-cell TDD systems," *IEEE Trans. Wireless Commun.*, vol. 10, no. 8, pp. 2640–2651, Jun. 2011

[14] F. Fernanders, A. Ashikhmin, and T. Marzetta, "Inter-cell interference in non-cooperative TDD large scale antenna systems," *IEEE J. Sel. Areas Commun.*, vol. 31, no. 2, pp. 192–201, Feb. 2013

[15] X. Zhu, Z. Wang, and L. Dai, "Smart pilot assignment for massive MIMO," *IEEE Commun. Letters*, vol. 19, no. 9, pp. 1644–1647, Mar. 2015

[16] M. Alkhaled, E. Alsusa, K. A. Hamdi, "Adaptive pilot allocation algorithm for pilot contamination mitigation in TDD massive MIMO systems," in Proc. IEEE Wireless Commun. and Networking Conf. (WCNC), Manchester, UK, 2017, pp. 1–6

[17] A. Ashikhmin and T. Maezetta, "Pilot contamination precoding in multi-cell large scale antenna systems," in Proc. IEEE International Symposium on Inform. Theory (ISIT), Cambridge, MA, USA, 2012, pp. 1137–1141

[18] A. Hu, T. Lv, H. Gao, Y. Lu *et al.*, "Pilot design for large-scale multi-cell multiuser MIMO systems," in Proc. ICC Conf., Budapest, Hungry, 2013, pp. 5381–5385

[19] S. Ni, J. Zhao, Y. Gong, "Optimal pilot design in massive MIMO systems based on channel estimation," *IET Commun.*, vol. 11, no. 7, pp. 975–984, May 2017

[20] L. S. Muppirisetty, H. Wymeersch, J. Karout *et al.*, "Location-Aided Pilot Contamination Elimination for Massive MIMO Systems," in Proc. Int. IEEE Global Communications Conf. (GLOBECOM), San Diego, CA, USA, 2015, pp. 1–5

[21] Z. Wang, P. Zhao, C. Qian *et al.*, "Location-Aware Channel Estimation Enhanced TDD Based Massive MIMO," *IEEE Access*, vol. 4, pp. 7828–7840, Nov. 2016

[22] H. Yin, D. Gesbert, M. Filippou *et al.*, "A Coordinated Approach to Channel

Estimation in Large-Scale Multiple-Antenna Systems," *IEEE Journal on Selected Areas in Communications*, vol. 31, pp. 264–273, Jan. 2013

[23] L. You, X. Gao, X. G. Xia *et al.*, "Pilot Reuse for Massive MIMO Transmission over Spatially Correlated Rayleigh Fading Channels," *IEEE Transactions on Wireless Communications*, vol. 14, pp. 3352–3366, Feb. 2015

[24] X. Zhu, L. Dai, and Z. Wang, "Graph Coloring Based Pilot Allocation to Mitigate Pilot Contamination for Multi-Cell Massive MIMO Systems," *IEEE Commun. Letters*, vol. 19, no. 10, pp. 1842–1845, Aug. 2015

[25] S. Uygungelen, A. Gunther, and B. Zubin, "Graph-based dynamic frequency reuse in femtocell networks," in Proc. IEEE VTC-Spring Conf., Yokohama, Japan, 2011, pp. 1–6

[26] K. Zheng, Y. Wang, C. Lin *et al.*, "Graph-based interference coordination scheme in orthogonal frequency-division multiplexing access femtocell networks," *IET Commun.*, vol. 5, no. 17, pp. 2533–2541, Nov. 2011

[27] J. Nam, A. Adhikary, J. Y. Ahn, and G. Caire, "Joint spatial division and multiplexing: Opportunistic beamforming, user grouping and simplified downlink scheduling," *IEEE J. Sel. Topics Signal Process*, pp. 876–890, Oct. 2014

[28] K. Yu and B. Ottersten, "Models for MIMO propagation channels: A review," *Wireless Commun. Mobile Comput.*, pp. 653–666, Nov. 2002

[29] M. Aslan and N. A. Baykan, "A Performance Comparison of Graph Coloring

Algorithms," in Int. Conf. on Advanced Technology and Sciences (ICAT), Konya, Turkey, 2016

[30] L. Lu, G. Y. Li, A. L. Swindlehurst, A. Ashikhmin, and R. Zhang, "An overivew of massive MIMO: Benefits and challenges," *IEEE J. Sel. Top. Signal Process.*, vol. 8, no. 5, pp. 742–758, Oct. 2014.

[31] X. Zhu, Z. Wang, C. Qian, L. Dai, J. Chen, S. Chen, and L. Hanzo, "Soft pilot reuse and multicell block diagonalization precoding for massive MIMO systems," *IEEE Trans. Veh. Technol.*, vol. 65, no. 5, pp. 3285–3298, May 2016.

[32] X. Zhu, L. Dai, Z. Wang, and X. Wang, "Weighted-graph-coloring-based pilot decontamination for multicell massive MIMO systems," *IEEE Trans. Veh. Technol.*, vol. 66, no. 3, pp. 2829–2834, Mar. 2017.

[33] H. T. Dao and S. Kim, "Vertex graph-coloring-based pilot assignment with location-based channel estimation for massive MIMO systems," *IEEE Access*, vol. 6, pp. 4599–4607, Jan. 2018.

[34] P. Liu, S. Jin, T. Jiang Q. Zhang, and M. Matthaiou, "Pilot power allocation through user grouping in multi-cell massive MIMO systems," *IEEE Trans. Commun.*, vol. 65, no. 4, pp. 1561–1574, Apr. 2017.

[35] H. Q. Ngo, M. Matthaiou, and E. G. Larsson, "Massive MIMO with optimal power and training duration allocation," *IEEE Wireless Commun. Lett.*, vol. 3, no. 6, pp. 605–608, Dec. 2014.

[36] X. Zheng, H. Zhang, W. Xu, and X. You, "Optimized pilot power allocation for

heterogeneous users in massive MIMO downlinks," in *Proc. IEEE ICTC*, Oct. 2014, pp. 246–250.

[37] Z. Xiang, M. Tao, and X. Wang, "Massive MIMO multicasting in noncooperative cellular networks," *IEEE J. Sel. Areas Commun.*, vol. 32, no. 6, pp. 1180–1193, Jun. 2014.

[38] H. V. Cheng, E. Bjornson, and E. G. Larsson, "Optimal pilot and payload power control in single-cell Massive MIMO systems," *IEEE Trans. Signal Process.*, vol. 65, no. 9, pp. 2363–2378, May. 2017.

[39] T. Wei, W. Feng, N. Ge, and J. Lu, "Optimized time-shifted pilots for maritime massive MIMO communication systems," in *Proc. Wireless and Optical Communication Conference WOCC*, NJ USA, May 2017.

[40] H. Al-Salihi, T. V. Chien, T. A. Le, and M. R. Nakhai, "A Successive Optimization Approach to Pilot Design for Multi-Cell Massive MIMO Systems," *IEEE Commun. Lett.*, vol. 22, no. 5, pp. 1086–1089, May. 2018.

[41] S. M. Kay, *Fundamentals of Statistical Signal Processing: Estimation Theory,* Upper Saddle River, NJ, USA: Prentice-Hall, 1993.

[42] D. Kong, D. Qu, K. Luo, and T. Jiang, "Channel estimation under staggered frame structure for massive MIMO system," *IEEE Trans. Wireless Commun.*, vol. 15, no. 2, pp. 1469–1479, Feb. 2016.

[43] M. Chang, *Geometric Programming for Communication Systems,* Hanover, MA, USA: now Publishers, 2005.

[44] J. Sturm, "Using SeDuMi 1.02, a MATLAB toolbox for optimization over symmetric cones," *Optimization Methods and Software*, pp. 625–653, Aug. 1998.

[45] R. K. Tutuncu and M. Todd, "Solving semidefinite quadratic-linear programs using SDPT3," *Mathematical Programming*, pp. 189–217, Sep. 2002.

[46] E. D. Andersen, B. Jensen, J. Jensen, and R. Sandvik, "MOSEK Verion 6," *Technical Report*, MOSEK, Sep. 2009.

[47] M. C. Grant and S. P. Boyd, "The CVX Users' Guide," *Release 2.1*, Dec. 2017.

[48] B. R. Marks and G. P. Wright, "A general inner approximation algorithm for nonconvex mathematical programs," *Operations Research*, vol. 26, no. 4, pp. 681–683, Aug. 1978.

[49] M. Chiang, C. W. Tan, D. P. Palomar, D. O. Neill, and D. Julian, "Power control by geometric programming," *IEEE Trans. Wireless Commun.*, vol. 6, no. 7, pp. 2640–2651, Jul. 2007.

[50] Z. Q. Luo and S. Zhang, "Dynamic spectrum management: Complexity and duality," *IEEE J. Sel. Topics Signal Process.*, vol. 2, no. 1, pp. 57–73, Feb. 2008.

[51] A. Tulino and S. Verdu, *Random Matrix Theory and Wireless Communications,* Hanover, MA, USA: now Publishers, 2004.

[52] E. Bjornson, J. Hoydis, and L. Sanguinetti, *Massive MIMO Networks: Spectral, Energy, and Hardware Efficiency,* NOW Publisher, 2017.

[53] T. V. Chien, E. Bjornson, and E. G. Larsson, "Joint pilot design and uplink power allocation in multi-cell massive MIMO systems," *IEEE Trans. Wireless Commun.*, vol. 17, no. 3, pp. 2000–2015, Mar. 2018.

[54] H. T. Dao and S. Kim, "Disjoint pilot power and data power allocation in multi-cell multi-user massive MIMO systems," *IEEE Access*, vol. 6, pp. 66513–66521, Oct. 2018.

[55] M. Mazrouei-Sebdani, W.A. Krzymien, and J. Melzer, "Massive MIMO with nonlinear precoding: Large-system analysis," *IEEE Trans. Veh. Technol.*, vol. 65, no. 4, pp. 2815–2820, Arp. 2016.

[56] Y. Han, Q. Liu, C.-K. Wen, M. Matthaiou, and X. Ma, "Tracking FDD massive MIMO downlink channel by exploiting delay and angular reciprocity," *IEEE J. Sel. Topics Signal Process.*, vol. 13, no. 5, pp. 1062–1076, Sep. 2019.

[57] T. V. Chien, E. Bjornson, and R. G. Larsson, "Joint power allocation and load balancing optimization for energy-efficient cell-free massive MIMO networks," *IEEE Trans. Wireless Commun.*, 2020, submitted. [Online]. Available: https://arxiv.org/abs/2002.01504

[58] P. Liu, K. Luo, D. Chen, and T. Jiang, "Spectral efficiency analysis of cell-free massive MIMO systems with zero-forcing detector," *IEEE Trans. Wireless Commun.*, vol. 19, no. 2, pp. 795–807, Feb. 2020.

[59] L. Sanguinetti, A. Zappone, and M. Debbah, "Deep learning power allocation in massive MIMO," in *Proc. Asilomar Conf.* , Oct. 2018.

[60] T. V. Chien, T. N. Canh, E. Bjornson, and E. Larsson, "Power control in cellular massive MIMO with varying user activity: A deep learning solution," *http://arxiv.org/abs/1901.03620*, 2019.

[61] T. V. Chien, C. Mollen, and R. Bjornson, "Large-scale-fading decoding in cellular massive MIMO systems with spatially correlated channels," *IEEE Trans. Commun.*, vol. 67, no. 4, pp. 2746–2762, Apr. 2019.

[62] T. V. Chien and E. Bjornson, *Massive MIMO Communications,* Springer International Publishing, pp. 77–116, 2017.

[63] J. Papandriopoulos and J. S. Evans, "SCALE: A low-complexity distributed protocol for spectrum balancing in multiuser DSL networks," *IEEE Trans. Inf. Theory*, vol. 55, no. 8 pp. 3711–3724, Aug. 2009.

[64] S. Boyd and L. Vandenberghe, *Convex Optimization,* Cambridge University Press, 2004.